Current Research (2018) Newfoundland and Labrador Department of Natural Resources
Geological Survey, Report 18-1, pages 31-57

THE APPLICATION AND TESTING OF TWO GEOPHYSICAL METHODS (DIRECT-CURRENT RESISTIVITY AND GROUND-PENETRATING RADAR) AS PART OF THE COASTAL MONITORING PROGRAM TO ASSESS TERRAIN STABILITY

G. Kilfoil, A. Blagdon[1], A. Leitch[1], H. Campbell, M. Irvine, M. Batterson, G. Roberts and B. Baker[1]
Terrain Sciences and Geoscience Data Management Section
[1]Department of Earth Sciences, Memorial University of Newfoundland, St. John's, NL, A1B 3X5

ABSTRACT

*Erosion of coastal cliffs of unconsolidated sediment is being studied by the Geological Survey of Newfoundland and Labrador as part of its coastal monitoring program. Currently, the monitoring program measures changes in morphology using high-resolution imagery, obtained using unmanned aerial vehicles (UAV). In 2017, geophysical methods were also employed as part of the ongoing interdisciplinary investigation of how physiochemical variations in subsurface sediments contribute to slope instability. Direct-current resistivity (DCR) and Ground-penetrating radar (GPR) were used to determine their effectiveness in delineating subsurface geology, in the communities of Daniel's Harbour and Parson's Pond on the Great Northern Peninsula. The results from the geophysical study were then compared to UAV imagery, and borehole and historical data. The DCR data successfully delineated subsurface geological layers, including the liquefaction-prone clay layer believed to be responsible for landslides in Daniel's Harbour. Although GPR was unable to image sediment layers at depth, the method was successful in capturing the structure of south-facing delta foresets in sediments at Parson's Pond. The DCR, in conjunction with other methods (*e.g.*, passive seismic surveys, single-shot seismic surveys), will be used in concealed (e.g., vegetation-covered) areas on the west coast in the future, to determine subsurface stratigraphy.*

INTRODUCTION

Coastal cliffs of unconsolidated sediments, along the west coast of the Great Northern Peninsula, Newfoundland and Labrador, have a history of landslides and ongoing coastal erosion, triggered by processes, such as vibration from heavy vehicle traffic, sudden loading (addition of mass), water saturation of sediment and subsequent liquefaction, and slope undercutting (*e.g.*, *see* Batterson *et al.*, 2006). Erosion is characterized by ongoing removal of material from cliffs due to wind and water (*e.g.*, Parson's Pond, Plate 1D), and landslides (*e.g.*, Daniel's Harbour, Plate 1B; south of Sally's Cove, Plate 1A). The proximity of some of these landslides to the highway, and the frequent occurrences of such slides (*e.g.*, Sally's Cove, December, 2017), reinforce the importance of ongoing coastal erosion studies. Thus, yearly monitoring is imperative, to understand erosion rates and to generate data that can be used by stakeholders for planning purposes.

PHYSIOGRAPHY

The regional terrain consists of extensive plains and wetlands, overlying a carbonate bedrock platform that extends from the crystalline basement escarpment of the Long Range Mountains to the coast (Knight, 1985; Cawood *et al.*, 1987; Owen, 1987; Williams and Cawood, 1989; Hinchey and Knight, 2011). Deep (600–700 m) fjords have been cut through the Long Range Mountains, leaving channels 600–1750 m wide, which now drain into large ponds near the coast (Figure 1).

OBJECTIVES

This study supports the multi-year coastal monitoring program on the west coast of Newfoundland (Irvine, 2012, 2013, 2014 and 2015) and it makes use of non-invasive geophysical methods and unmanned aerial-vehicle (UAV) imagery to identify subsurface geological features susceptible to slope failure. The geophysical objective was to differentiate unconsolidated sedimentary layers of differing composition and grain sizes, based on contrasting electrical properties, using Direct-current resistivity (DCR) and Ground-penetrating radar (GPR). The GPR has previously been used effectively in the delineation of Quaternary sediments in Newfoundland (McCuaig, 2006) and Finland and Alaska (*e.g.*, Sutinen, 1992; Murray and Booth, 2010), and DCR has been used to characterize glacial sediments in

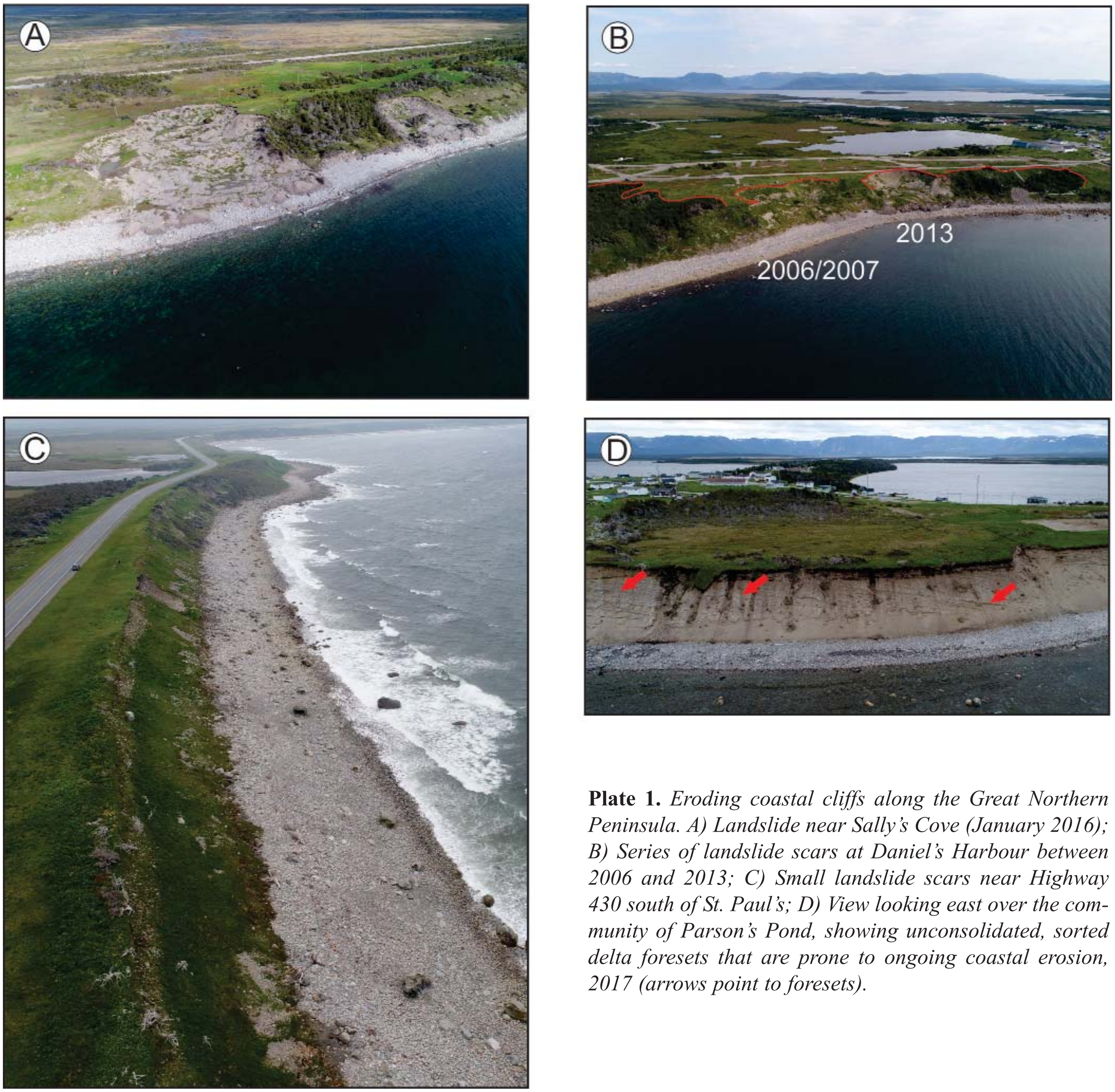

Plate 1. *Eroding coastal cliffs along the Great Northern Peninsula. A) Landslide near Sally's Cove (January 2016); B) Series of landslide scars at Daniel's Harbour between 2006 and 2013; C) Small landslide scars near Highway 430 south of St. Paul's; D) View looking east over the community of Parson's Pond, showing unconsolidated, sorted delta foresets that are prone to ongoing coastal erosion, 2017 (arrows point to foresets).*

Sweden and Norway (*e.g.*, Lundstrom *et al.*, 2009; Donohue *et al.*, 2012).

The communities of Daniel's Harbour and Parson's Pond were chosen to determine the effectiveness of GPR and DCR in delineating subsurface discontinuities, as each of these communities appears to be underlain by unconsolidated sediments of differing grain sizes, including massive unsorted glacial sediments of Daniel's Harbour and sorted sediments at Parson's Pond. Systematic UAV images were acquired, to provide accurate surface elevation information and updated imagery for sediment stratigraphic mapping, and for comparison with earlier/previous UAV surveys.

The study aims to:

1) Develop efficient, non-destructive and inexpensive methods to determine areas vulnerable to slope movement;
2) Determine the factors affecting terrain instability in unconsolidated sediments; and
3) Build a terrain-hazard map from these data.

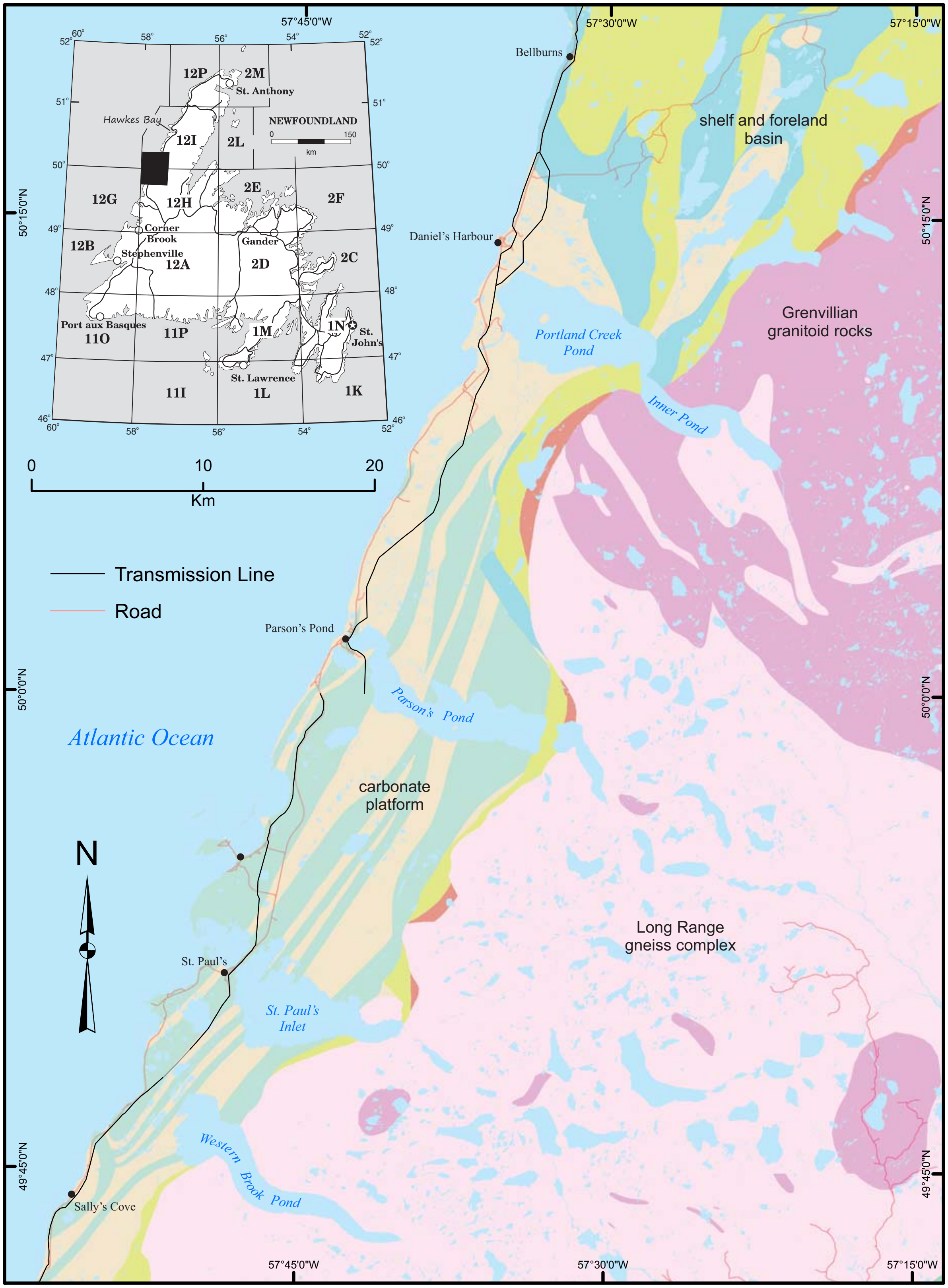

Figure 1. *General bedrock geology map of the study area (Knight, 1985; Cawood* et al.*, 1987; Owen, 1987; Williams and Cawood, 1989; Hinchey and Knight, 2011). Drainage is east to west from the highlands of the Long Range Mountains (pink units) over the carbonate platform (yellow and green).*

STUDY AREAS

INTRODUCTION

Two study sites with good, independently acquired knowledge (Jacques Whitford, 2006, 2008) of surficial stratigraphy (*e.g.*, boreholes, coastal exposure) were studied. Daniel's Harbour and Parson's Pond (Figures 1 and 2) are located along the Viking Trail (Highway 430), the only land-transportation link for communities on the Great Northern Peninsula (Table 1). Hydroelectric power lines are located along this route, and both the power lines and the highway,

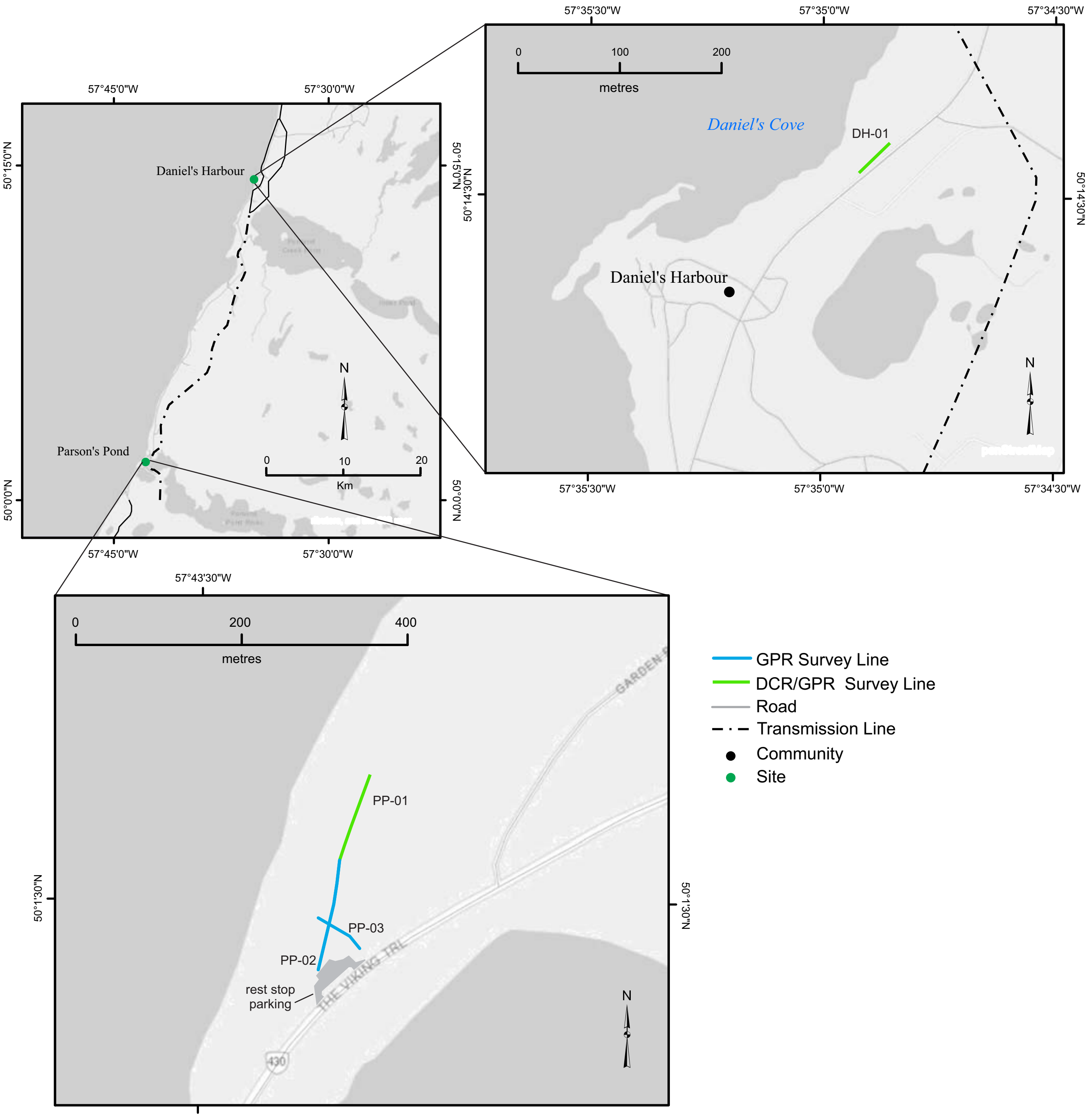

Figure 2. *Maps showing locations of the Daniel's Harbour and Parson's Pond field sites. The Daniel's Harbour landslide site (upper right), and an eroding unconsolidated coastal cliff in the community of Parson's Pond (lower left). The blue and green lines show the locations of DCR and GPR survey lines.*

Table 1. Location coordinates for geophysical survey lines included in this study. Field site abbreviations are: DH – Daniel's Harbour; PP – Parson's Pond

Line No.	UTM Coordinates* Start	End	Length (m)	No. of stations	Geophysical Methods
DH-01	458578.8 E 5565803.5 N	458495.9 E 5565723.8 N	115	24	DCR & GPR
PP-01	448276.8 E 5541818.3 N	448238.3 E 5541710.0 N	115	24	DCR & GPR
PP-02	448238.3 E 5541710.0 N	448212.5 E 5541577.8 N	135	5	GPR only
PP-03	448263.9 E 5541600.0 N	448212.7 E 5541638.8 N	64	3	GPR only

* NAD 83, UTM Zone 21 U

excluding the section relocated due to the landslides in Daniel's Harbour, are within 100 m of the coastline in several places (*e.g.*, south of St. Paul's, and at Sally's Cove).

The town of Daniel's Harbour (Figure 2) is located on a gently sloping hill leading to a marine terrace 25 m above sea level. The Daniel's Harbour site is located within the fenced-off area adjacent to the 2006, 2007 and 2013 landslides. This site also shows evidence of previous slope instability (*e.g.*, arcuate scars on the coastline, fissures on the surface) to the north and south of the recent slides.

The town of Parson's Pond is on a terrace 25 m above sea level, in an area underlain by sandier sediments than at Daniel's Harbour. The study site (Figure 2) is situated on level ground on top of a coastal cliff that is being subject to active steady-state erosion, as opposed to a combination of steady-state and catastrophic erosion that has prevailed at the Daniel's Harbour site.

Daniel's Harbour

At Daniel's Harbour, on October 20, 2006, there was a small landslide that covered an area of approximately 0.1 hectares (1000 m^2; Plate 1B). Another landslide occurred on April 15, 2007, involving an area of at least 0.53 hectares (5300 m^2) and displacing about 110 000 m^3 of material (Plate 1B). This landslide resulted in significant loss of property, including several residences, the subsequent removal of other buildings from the site, and the eventual relocation of 23 properties. In June 2008, a smaller landslide, 20 m wide and 7 m high, occurred 220 m south of the 2007 landslide. In 2013, another landslide, extending the landslide scar landward to the old highway, occurred about 20 m southwest of the 2007 landslide. Portions of the old highway collapsed a few days later (Plate 1B), and a water-supply pipe was subsequently relocated.

The glacial sediments of the landslides were studied in boreholes drilled at Daniel's Harbour and detailed in a report by Jacques Whitford (2006). Studies of soil-moisture content, and grain-size analysis of each layer, are summarized in Table 2; a 3-D representation of the 2007 landslide intersected by the boreholes is given in Figure 3 and a sedimentary profile illustrated in Figure 4. Descriptions of the four sedimentary layers are as follows:

Table 2. Summary of the characteristics of unconsolidated sediment encountered in boreholes at Daniel's Harbour (Jacques Whitford, 2006)

Material (defined by engineering properties)	Avg. Gravel %	Avg. Sand %	Avg. Silt and Clay %	Avg. moisture conent %	Thickness Range (m)	Interpreted Genesis	Borehole Code
Organic soil	NA	NA	NA	NA	0.6-3	Post glacial-organic accumulation	OL
Loose sand and gravel	NA	NA	NA	NA	2-4	Marine veneer (nearshore sediments)	SM
Compact to dense grey, silty clayey-sand	15.2	41.5	43.3	9.3	11-26	Marine diamicton (till)	SC-SM
Loose to compact clayey-sand with gravel - occasional cobbles	18.1	38.7	43.1	10.8	1-12	Marine diamicton or marine debris (melt-out?) emplaced in an ice-proximal marine environment	SC
Grey sandy lean clay	8.8	22.7	68.5	17.6	0.3-3	Marine – sediments deposited by settling in quiescent waters	CL

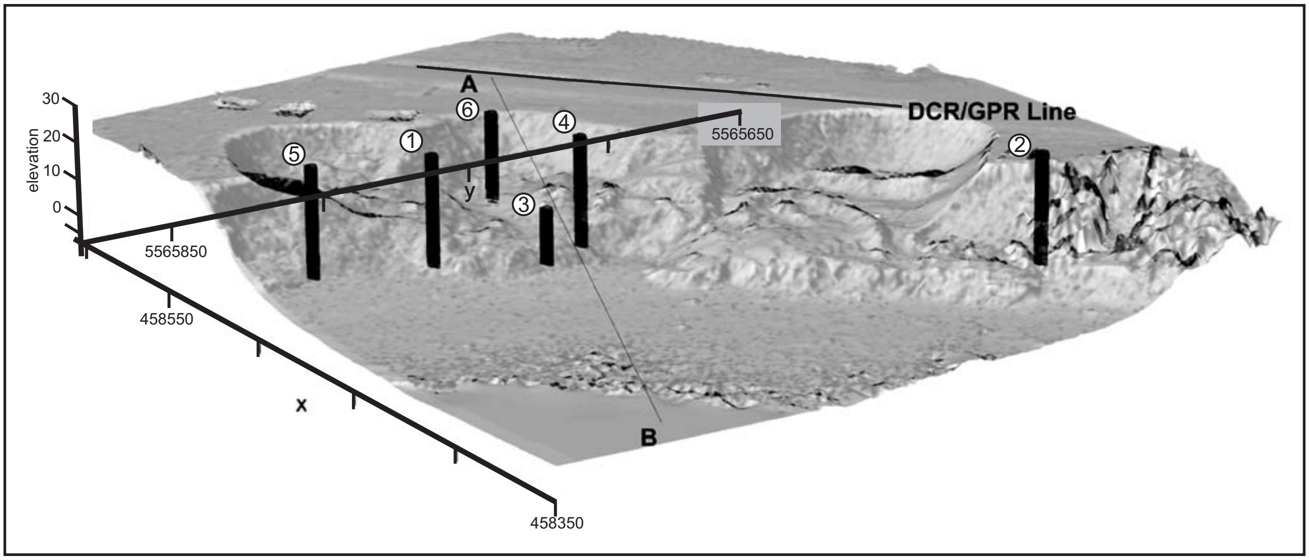

Figure 3. *Location of boreholes in the Daniel's Harbour landslide, superimposed on the DSM produced from the 2017 UAV survey. The boreholes were drilled in 2006 prior to the 2007 landslide (scar surrounding boreholes 1, 3, 4, 5 and 6) and the 2013 landslide (scar to the left of borehole 2). Location is defined by the UTM coordinates (NAD 83, UTM Zone 21N; X = easting, Y = northing); elevation above sea level is denoted by the Z axis; the trace of the section (Figure 4) is denoted by line A-B.*

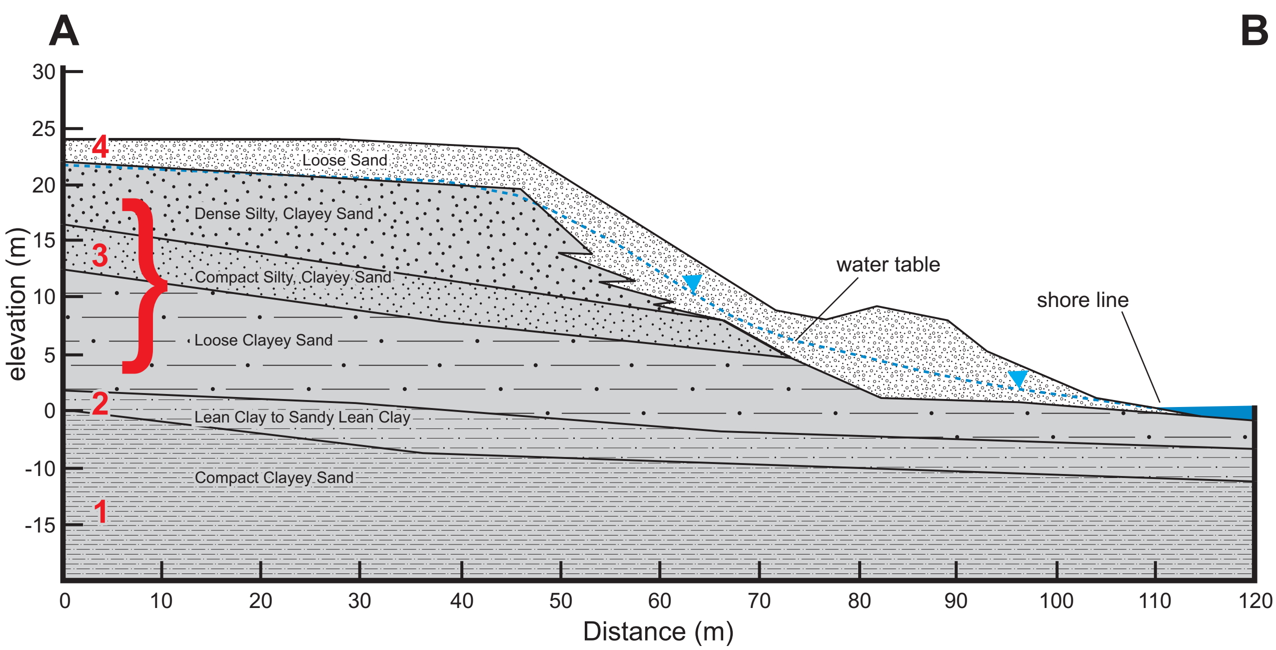

Figure 4. *Section showing representative glacial stratigraphy at Daniel's Harbour (Jacques Whitford, 2006). The sediments were initially separated on the basis of engineering properties, and have been interpreted as four distinct glacial stratigraphic units (in red).*

Unit 1 – The lowermost unit (encountered only in boreholes) is a compact, grey clayey sand with gravel and a few cobbles whose thickness is unknown. This unit is interpreted as a diamicton.

Unit 2 – This unit is a layer of compact, grey, sandy clay, 2.0 to 3.2 m thick.

Unit 3 – The grey sandy-clay layer is overlain by 10 m of loose clayey sand grading into 10 m of compact silty-grey, clayey sand with gravel and a few cobbles. This unit is well exposed in coastal cliffs, and includes shell fragments. It contains striated clasts derived from the Long Range Mountains to the east, and from the carbonate rocks that underlie the study area (M. Batterson and P. Deering, personal communication, 2017), and is interpreted as a glaciomarine diamicton.

Unit 4 – The subsurface layer is a weakly stratified, loose sand and gravel layer (approximately 2 to 3 m thick) that overlies the glaciomarine diamicton along a sharp, planar contact.

The causes of the landslide at Daniel's Harbour were both a 'translational slip failure' and a 'rotational slip failure', that occurred as the result of saturation and subsequent seaward movement of the layer of grey, sandy clay (Unit 2), underlying the glaciomarine diamicton (Unit 3) (M. Batterson and P. Deering, personal communication, 2017).

Parson's Pond

Horizontal retreat of unconsolidated coastal cliffs at Parson's Pond has been occurring at an average rate of 73 cm per year. Surface and groundwater erosion are observed in gully and rill development on cliff faces; notching along the base of the cliff indicates wave erosion (Irvine, 2015). The ongoing erosion of material present less of a threat to infrastructure. However, the proximity of vital infrastructure (*e.g.*, hydroelectric power lines, roads) is an issue.

The UAV photos of the cliff faces at Parson's Pond (Plates 2 and 3) were used to determine stratigraphy. The sediment succession is described starting from the beach, and ending with the uppermost (surface) unit; there are four units:

Unit 1 – Beds of fine sand and gravel with an apparent dip of 20° southward; north of the study area the apparent dip of the beds is 40° northward.

Unit 2 – An isolated diamicton lens having a cobble base is enveloped by beds of sand and gravel.

Unit 3 – A 3-m-thick planar unit overlies the dipping stratified beds (Unit 1) in the southern portion of the cliff; this unit fines upward, with cobbles and gravel at the base, and laminated sands with minor silt and clay toward the top.

Unit 4 – Dipping beds (Unit 1) are truncated to the north by a 5- to 8-m-thick ridge composed of cobble and gravel-rich material with some clay (Plate 2).

METHODS

UNMANNED AERIAL VEHICLE (UAV)

A quadcopter UAV was flown over the Daniel's Harbour and Parson's Pond sites in 2016 and 2017 (Table 3). In 2017, the UAV was upgraded from the DJ Inspire 1 to the next version, the DJ Inspire 2; improvements include a camera with greater resolution, longer flight time, faster flying speed and improved obstacle avoidance. Traverses were designed using the Maps Made Easy web application and flown on auto-pilot, with an 80% image overlap and a vertically oriented camera. Manual mode was used to capture oblique photographs. Photos were acquired during periods of minimal wind speed (below 25 km/h), and an hour after sunrise and before sunset, to ensure there were sufficient levels of daylight.

Prior to each flight, ground-control points (GCPs), consisting of 30 cm by 30 cm black and white targets, mounted on plywood and readily discernible in the images, were placed on flat ground. A Leica GS09 RTK system with sub-

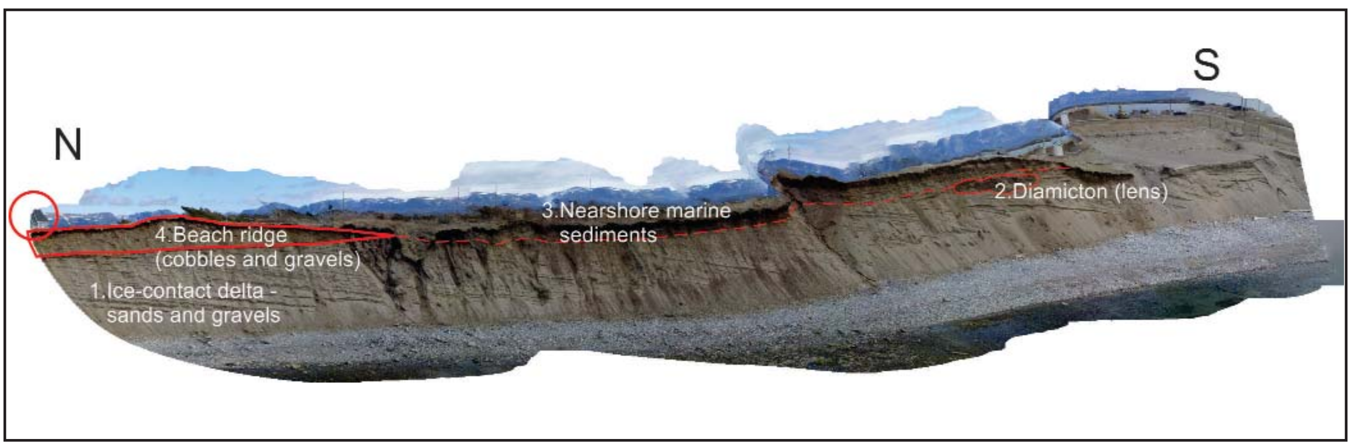

Plate 2. *Oblique view of the cliff at Parson's Pond, taken from the UAV, looking east from the coast toward the Long Range Mountains (the circled house on the left is 5 m high). A gently dipping, sand and gravel sequence is interpreted as an ice-contact delta (1) that encompasses a lens of clay, cobble and gravel; interpreted as ice-contact diamicton (2). This sequence is overlain by planar, stratified sands and silts (3); interpreted as having been deposited in a nearshore marine environment. The raised feature north of the profile (4) is probably a beach ridge, deposited during a period of elevated sea level.*

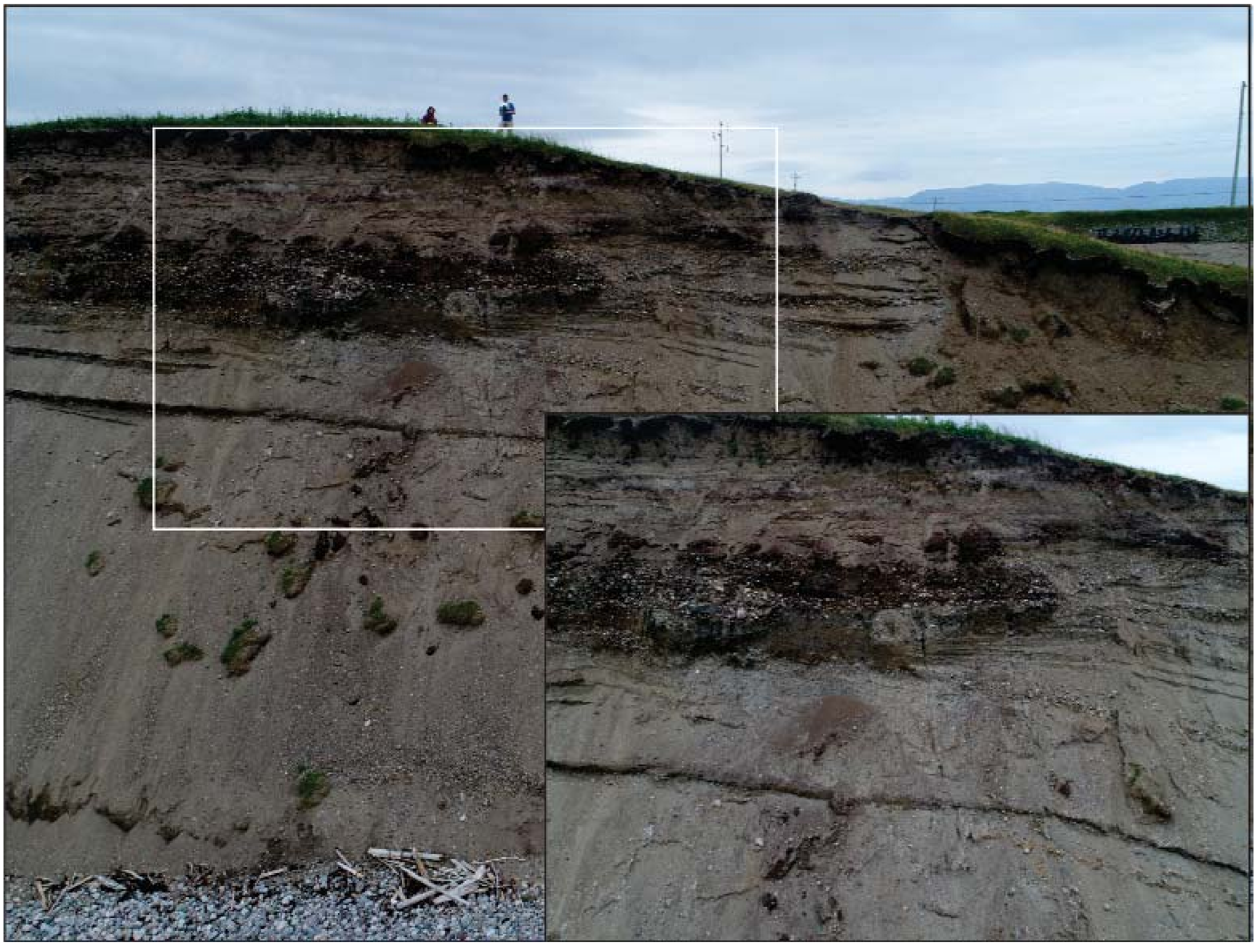

Plate 3. *Diamicton lens (person is 1.5 m tall); with coarser grained sediments deposited over finer grained gently dipping sand and gravel layers.*

Table 3. Summary statistics for the 2016 and 2017 UAV flights at Daniel's Harbour and Parson's Pond. The combination of flight altitude and camera focal length resulted in higher ground resolution in 2017 compared to 2016

	Daniel's Harbour 2016	Daniel's Harbour 2017	Parson's Pond 2016	Parson's Pond 2017
UAV	DJI Inspire 1	DJI Inspire 2	DJI Inspire 1	DJI Inspire 2
Flying altitude (m)	83.1	67.7	72	42.2
Number of Ground Control Points (GCPs)	6	6	5	9
Ground resolution* (cm)	2.97	1.5	2.58	1.05

* the distance between the centres of two neighbouring pixels

centimetre accuracy, operating in survey mode, was used to obtain the exact locations of the centre points of the targets.

PHOTOGRAMMETRY

The UAV data were processed using Agisoft Photoscan Professional software that implements the photogrammetric technique 'Structure from Motion' (SfM). The SfM enables the construction of 3-D imagery from 2-D photographs, using algorithms to detect matching points between images (Westoby *et al.*, 2012). This study used methods described in Irvine *et al.* (*this volume*). A Digital Surface Model (DSM), an orthophotograph, and a 3-D model were derived for the landslide scars at Daniel's Harbour (Figure 5), and of the unconsolidated coastal cliff at Parson's Pond.

To quantify topographic changes in the landslide scars and cliff face, the DSM from 2017 was subtracted from that of 2016 for Daniel's Harbour and Parson's Pond. Elevation changes are represented by a colour-coded scale indicating the amount of change. In assigning colours, the data are sort-

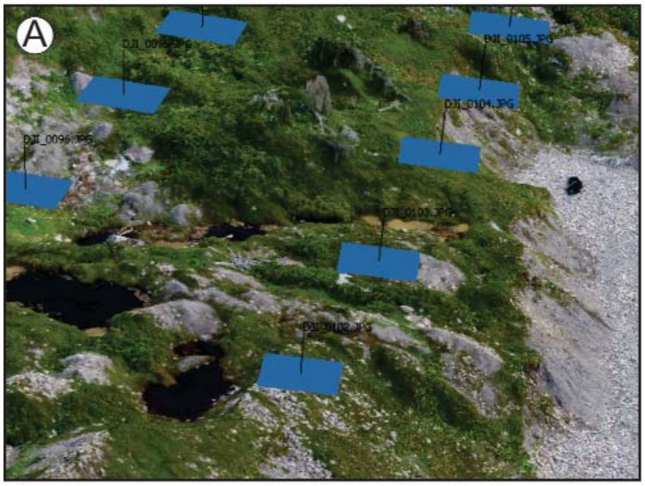

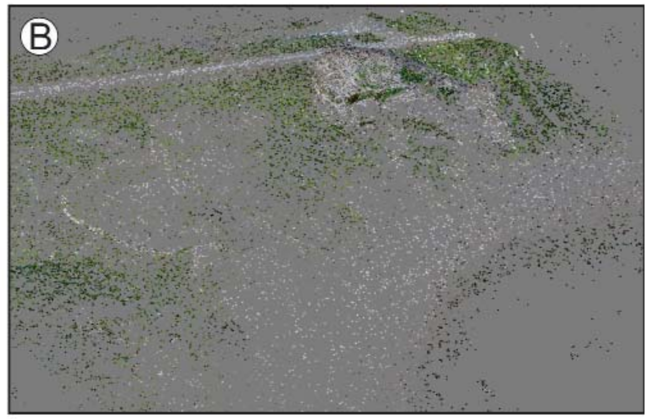

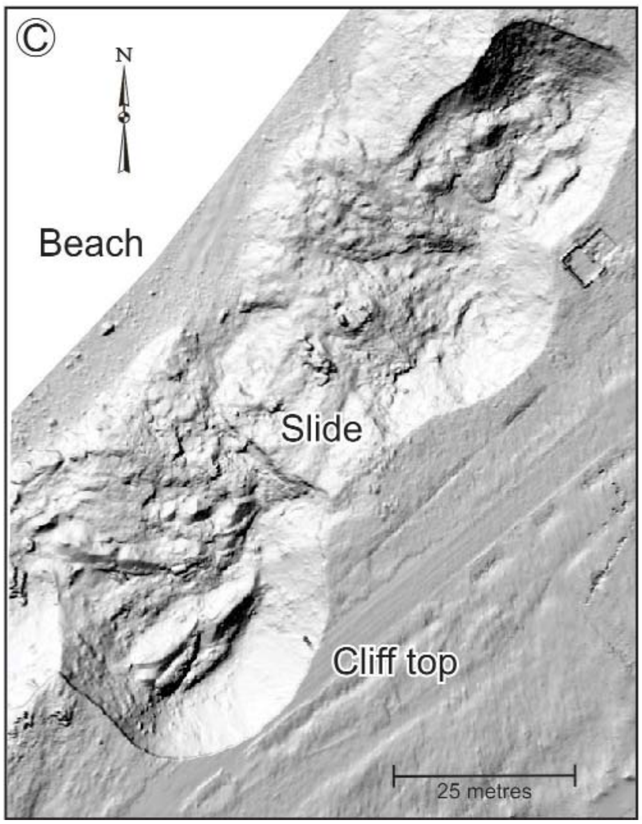

Figure 5. *Plates illustrating the photogrammetry acquired in the Daniel's Harbour area. A) Partial view of the textured 3-D surface of the coastal cliff, taken in 2017. The blue rectangles show the positions of the photographs captured by the UAV, and the black lines the directions in which they were taken; B) Oblique view of the point cloud created from the 2017 imagery; C) Close-up map view of a greyscale representation of the DSM, with the sun's relative position taken into account for shading; D) A 3-D model of the coastline in the vicinity of the 2006, 2007 and 2013 landslides, created from the 2017 UAV data (oblique view, looking southeast) for B and D.*

ed into classes, each representing an interval of 20 cm of change; this classification interval is greater than the estimated error in UAV data accuracy and ground resolution, and is an optimal value for displaying data trends for this study.

GEOPHYSICS

DCR

Direct-current resistivity (DCR) exploits variations in the electric resistivity (the reciprocal of conductivity) of geological materials to "image" subsurface geology (Reynolds, 1997, Chapter 7). In this method, an electric current is applied between one outer pair of current electrodes, and the electrical potential (voltage) is measured across an inner pair of potential electrodes (Figure 6), to determine the apparent resistivity of the subsurface within the electrode span, using Ohm's Law. This arrangement of four electrodes, installed in the ground, is referred to as an "array". Apparent resistivity is a weighted average of the resistivities of the material through which the current flows. For uniform ground and constant input current, the measured potential is

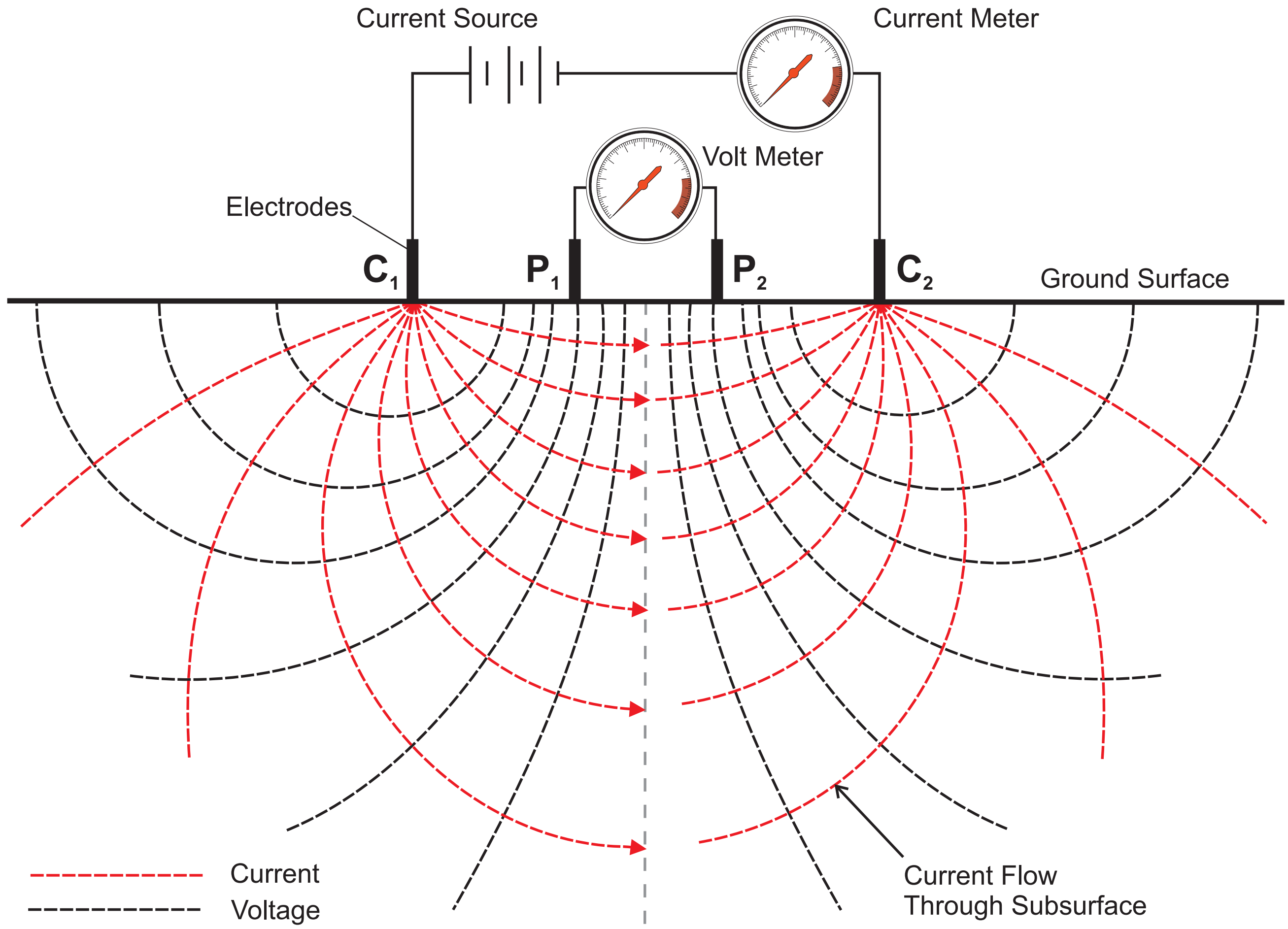

Figure 6. *Diagram of a general DCR array showing the relative positions of a symmetrically arranged pair of current electrodes (C_1 and C_2) and a pair of potential electrodes (P_1 and P_2). Also shown are resulting current flow lines (marked with red arrows) and equipotentials (dotted lines) in a homogeneous subsurface (Sharma, 1997).*

proportional to the resistivity of the ground; a smaller measured potential would be recorded over a conductive subsurface, and a larger measured potential would be recorded over more resistive layers. For plotting, the location of the measurement is in the centre of the array at a depth approximately equal to half the width of the electrode span. The investigation depth increases with current electrode spacing, so that measurements recorded at successively wider electrode spacings enable a resistivity-depth profile to be constructed. By moving the array along a survey line and combining results for varying electrode spacings, a 'pseudo-section' of apparent resistivity may be constructed. The signal-to-noise ratio decreases (and therefore uncertainty increases) with depth, as the input current is diluted over a larger volume.

Two common electrode configurations used in DCR are the Wenner, and Schlumberger arrays. Both use symmetrical arrangements where the electrodes are placed in a straight line: the Wenner array, favoured for profiling in the horizontal, the spacings between all electrodes (the 'a' spacing) is constant; for the Schlumberger array, favoured for depth soundings, the 'b' spacing between the potential electrodes is kept constant while the current electrode spacing is increased (*see* Reynolds, 1997).

Induced Polarization (IP) surveys can be included in DCR surveys. In IP surveys, the 'capacitance' of the ground is measured by recording the decay of the potential after the current is switched off. This measurement can be useful in detecting high clay content, as clay minerals behave like tiny capacitors in the subsurface, which generates an IP response.

GPR

With Ground-penetrating radar (GPR), an electromagnetic (EM) pulse is projected downward into the ground from a transmitting antenna. Where interfaces between media of contrasting dielectric properties (electric conductivity, electric permittivity and magnetic permeability) exist in the subsurface, part of the signal is reflected back toward the surface (according to Fresnel's equations; Griffiths, 2013, pages 409-411) where it is detected by a receiver antenna (Figure 7). The GPR equipment records the amplitudes of the reflected energy and the times of arrival, which are the two-way travel times of the radar pulse's pathway through the subsurface. Significant and abrupt changes in the dielectric properties at an interface generate high-amplitude reflections in the recorded data. The response from one radar pulse is called a "trace". A GPR profile, made up of a sequence of traces, is generated as the two antennae are moved together along a survey line, as illustrated in Figure 7.

To convert two-way travel times to depth, it is necessary to know the wave velocity through the ground. A typical, default velocity for near-surface sediments is 0.1 m/ns (Sensors and Software Inc., 2006), about one-third the speed of light in a vacuum. An isolated body (such as a boulder) produces a hyperbolic reflection pattern in a GPR profile (*ibid.*). An automated tool in the GPR software allows the velocity to be estimated from the shape of the reflection hyperbola.

The GPR is analogous in concept to seismic-reflection methods. The major differences between radar and reflec-

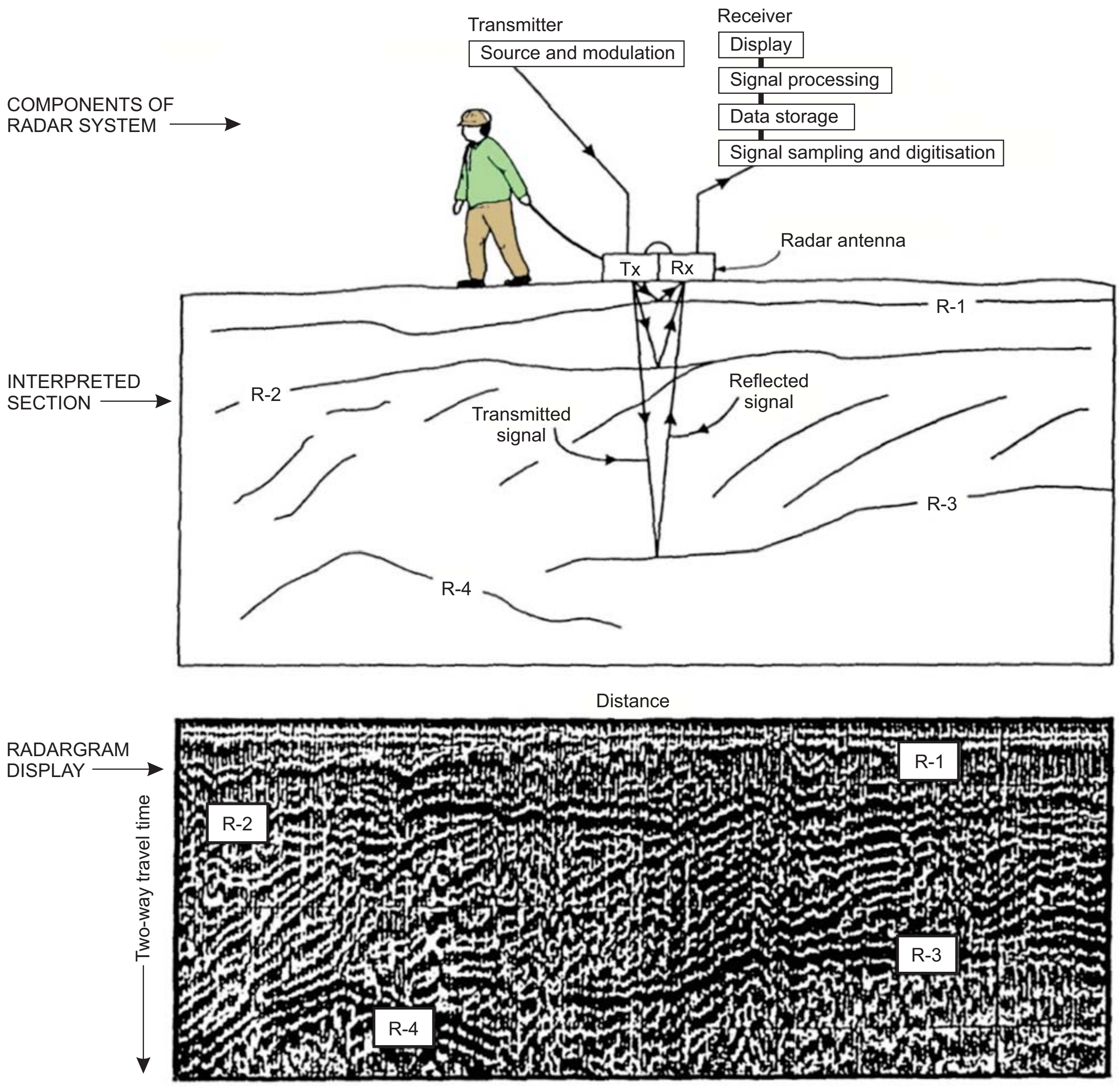

Figure 7. *Diagram illustrating the principles of GPR surveying (from Reynolds, 1997). As the source pulse consists of a short wavelet with 3 or 4 peaks, reflectors R-1 to R-4 in the interpreted section show up as several dark and light bands in the radargram display.*

tion seismic are that a radar pulse, rather than a sonic pulse, is used as a signal source, so that reflections occur from changes in dielectric properties rather than acoustic properties. Also, a single receiver (the receiver antenna) is used rather than an array of geophones. Seismic signals have frequencies of 10s to 100s of Hertz, whereas the radar frequencies are several orders of magnitude higher – 10s to 100s of megahertz (MHz). At such ultra-high frequencies, radar can provide excellent spatial resolution of buried objects in the near surface, but the trade-off is that depth penetration is much less than seismic surveys can typically provide. The penetration depth for radar depends on the radar pulse (and tuned antennae) frequency and the ground conditions: nominal depths for the 100 and 50 MHz antennae used in this study are 5 and 10 m, respectively (Sensors and Software Inc., 2006). However, these depths can be significantly reduced due to energy scattering from near-surface cobbles, and signal attenuation due to a conductive subsurface, such as salt- or clay-rich sediments. The GPR method works best in relatively resistive ground, where grain-size variations are less than the radar pulse wavelength (a few centimetres) and where the reflecting interfaces are close to normal to the signal (*i.e.*, in horizontal to gently dipping layered ground).

SURVEY SETUP

The DCR and GPR surveys were carried out along profile lines, approximately 115 m long, at the Daniel's Harbour and Parson's Pond sites (Figure 2, Table 1). The lines are referred to by DH and PP designations, respectively, in this paper. Plate 4 shows the geophysical equipment deployed during this study.

The DCR and GPR responses can vary greatly, depending on the geometry and physical properties of subsurface media. The GPR method should effectively image homogeneous lenses of gravel and sand having horizontal to gently sloping interfaces, such as are present at Parson's Pond. Resistivity surveys are effective at imaging layers of contrasting electrical properties such as the sandy marine sediments over clay-rich diamicton at Daniel's Harbour. Small changes in the relative proportions of silica sand (containing electrically resistive quartz) and clay (which contains electrically conductive phyllosilicate minerals) cause significant changes in apparent resistivities. Thus, the electrical contrast between the siliceous marine sandy veneers and underlying clay-rich diamicton should be detectable by this survey method.

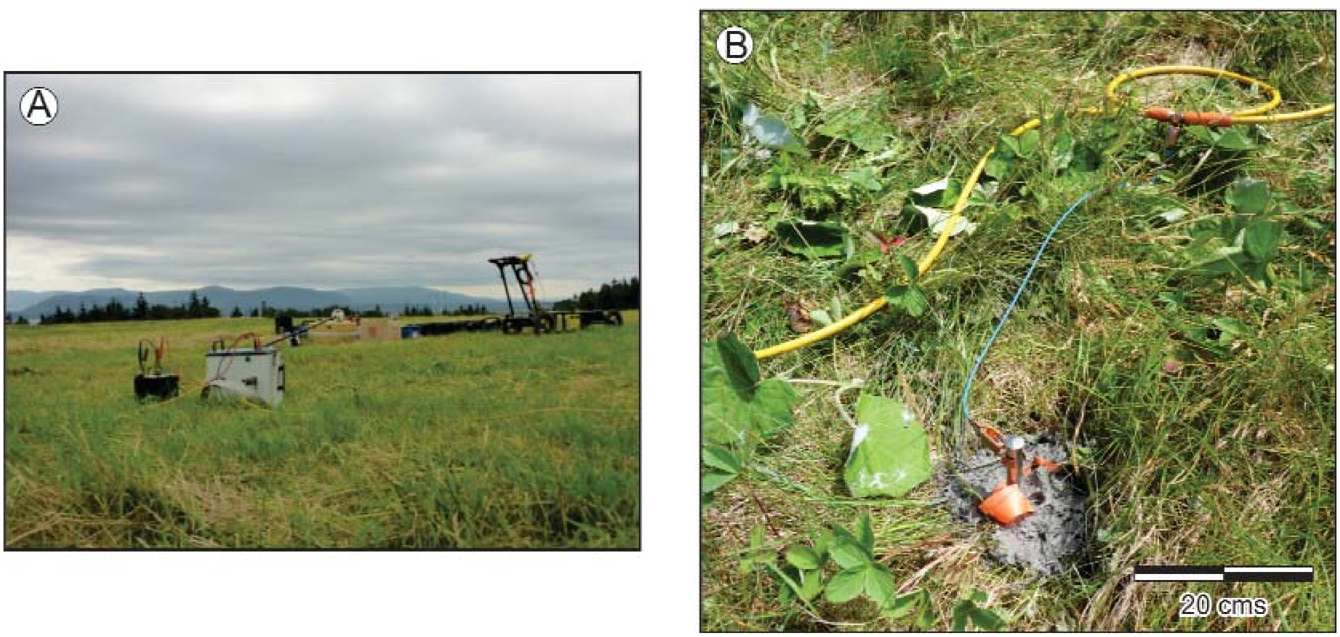

Plate 4. *A) Photo of a field site, showing geophysical equipment. The grey box in the foreground is the DCR console, which is connected to an external battery (black box) for power, and to two multicore recording cables, to which the electrodes are attached. Farther back is the GPR instrumentation, mounted in a SmartCart trolley; B) Close-up view of equipment set up at an electrode location. The top portion of an electrode, identified by orange flagging tape, is connected to the multicore recording cable (yellow) by a jumper wire (pale blue). A clay-water slurry (grey material at the electrode) was added to the ground surrounding this electrode to reduce its electrical contact resistance.*

In this study, an IRIS Syscal Junior DCR system with multicore cables was used. This system allows 24 electrodes to be deployed, and can be programmed to take a sequence of measurements of resistivity (and IP) using various electrode positions and spacings as illustrated in Figure 8, so that an image of the subsurface apparent resistivity distribution can be produced. This pseudo-section can then be modelled using specialized software RES2DINV (Geotomo, 2017) to generate a depth section of the real resistivity.

At the Daniel's Harbour site, previous studies in 2006 had identified a clay-rich unit, at a depth of about 20–25 m, as a potentially important feature in cliff failure. Hence, in this study the 24 electrodes were spaced at 5 m intervals, to enable resistivity models to be produced to depths of approximately 25 m near the centre of the electrode spread.

The GPR system used was a Sensors and Software pulseEKKO PRO, mounted on a wheeled Smartcart with 100 MHz and 50 MHz antennae.

At both study sites, the survey lines were located on relatively level, uniform ground. Plastic tent pegs were first driven into the ground at 5 m intervals along a straight line to mark DCR electrode locations. Following the DCR survey, the metal electrodes were removed but the plastic pegs remained, allowing the electrode sites to be identified during the subsequent GPR survey, and for the purpose of georeferencing with a Real Time Kinetic (RTK) GPS system.

The DCR utilized 30-cm stainless-steel electrodes, which were driven into the ground to a depth of 25 cm and connected by alligator clips to multicore cables. The cables were then connected to the IRIS Instruments Syscal Junior DCR unit. The contact resistance at each electrode was checked to ensure good ground contact. At the Daniel's Harbour site, the electrode contact resistance was found to be very high, due to the presence of highly resistive loose gravel at the surface and very thin to patchy soil development. To address this, clay from the nearby cliff was mixed with water and this slurry was packed around each electrode to increase contact with the surficial materials, and effectively couple the electrodes to the ground (Plate 4B). The substrate in the near surface at Parson's Pond was sufficiently uniform and conductive that clay was not required to improve the electrode/ground contact.

The DCR unit was pre-programmed to acquire apparent resistivity and IP data in the desired array sequence. During the recording sequence, which lasted about three hours, the unit automatically cycled through all possible arrays within the electrode spread (*see* Figure 8).

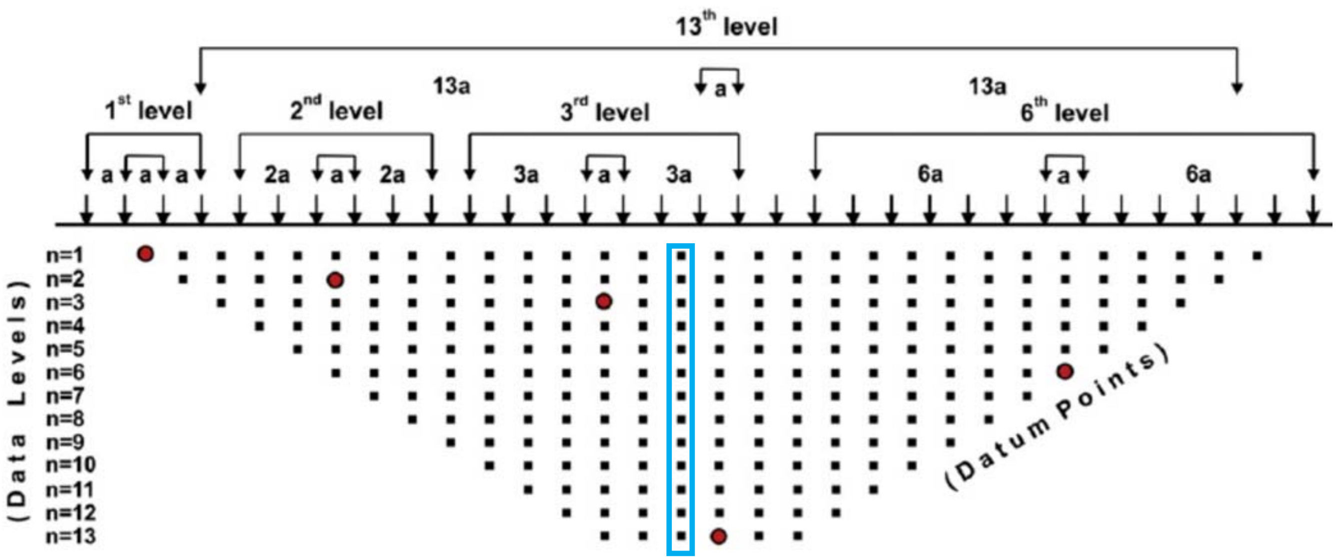

Figure 8. *Schematic diagram of a DCR Wenner-Schlumberger array sequence (modified after Levent Ekinci* et al*., 2013). Electrode locations are marked by arrows touching the continuous horizontal line representing the ground surface. The data levels (indicative of pseudo-depth) are based on the width of the electrode arrays. The square dots show the plotting locations for an entire sequence of measurements involving 13 levels. All measurements are required to build up a pseudo-section of apparent resistivity. The red dots, from left to right, highlight the plotting location of measurements taken by arrays labelled 1st level, 2nd level, 3rd level, 13th level and 6th level, respectively. The blue rectangle encloses data values that could be used in a vertical electric sounding (*see *text) (Cooper, 2000).*

PROCESSING

The GPR and DCR results, and the models generated from them, are generally presented as X-Z profiles, depth sections or pseudo-sections, where X is the horizontal coordinate representing the distance or position along a survey line, and Z is the vertical coordinate representing the depth within the ground. The z-coordinates can either be plotted as the depth beneath the surface (increasing downward) or as elevation (increasing upward). In this paper, depth beneath the surface was used universally, as, although the DCR survey lines were situated on level ground, certain GPR traverses were situated over significant topographic relief resulting in severe distortion of the profile presentations. Features observed in the results and discussed are identified by their x- and z-coordinate locations, unless highlighted in the presentations.

Raw DCR apparent-resistivity data were first smoothed using a weighted 3-point average to remove the effects of small-scale surface heterogeneities (Lane *et al.*, 1995) and plotted as pseudo-sections. The smoothed data were inverted using a least-squares algorithm in Geotomo's (2017) RES2DINV software. RES2DINV sets up a grid of rectangular cells and calculates the best-fit resistivities at cell centres that would satisfy the recorded values within an optimal misfit range.

In addition to the smoothed sections produced by RES2DINV, "vertical electric soundings" (VES) were extracted from the apparent-resistivity data. To create a sounding, apparent-resistivity data at a specific "x" location along the profile and all pseudo-depths at that surface location (the blue rectangle in Figure 8 outlines the data used for one such sounding) were inverted using the freeware VES application (Cooper, 2000), to yield a profile of resistivity versus depth. The VES modelling assumes a one-dimensional stratigraphy of a finite number of layers with constant properties, and sharp interfaces between them.

Sensors and Software's affiliated GPR processing software Ekko Project, compatible with the pulseEKKO Pro equipment used at the Daniel's Harbour and Parson's Pond field sites, was used in the data processing of all GPR survey lines completed.

Initially, the Average Frequency Spectrum plot of each of the GPR profiles was analyzed to ensure the dataset is not contaminated with low-frequency noise associated with proximity to transmission lines near each of the sites. Such artifacts can be removed effectively by applying a high-pass filter available in Ekko Project (Sensors and Software Inc., 2006).

The saturation of the recorded GPR signal by early reflection arrivals, caused by proximity of the transmitter and receiver and/or inductive coupling effects between the ground and antennae, is termed the "wow" effect. A "dewow" filter was automatically applied to each GPR profile to correct for DC bias and to remove this saturation of very low-frequency components of signal in each of the traces (Jol, 2009; Szymczyk and Szymczyk, 2013). A background subtraction filter was also used to remove the horizontal banding (at early arrival times) present throughout GPR profiles due to the interaction of the direct air and ground waves with the receiving antennae (Sensors and Software Inc., 2017).

Ekko Project's "Hyperbola Velocity Calibration" tool was used to calculate the speeds of the radar pulses in the uppermost subsurface layers at both field sites, verifying that the assigned velocities were reasonable values (Sensors and Software Inc., 2017). Each of the GPR profiles were truncated at t=100 ns, as the signal had become completely attenuated beyond that two-way travel time value.

RESULTS OF UAV STUDIES

DANIEL'S HARBOUR

2013 Landslide

Between 2016 and 2017, sediment eroded from the base of the 2013 landslide scar (Figure 9). It is probable that this erosion occurred as a result of wave action during storms when the cliff face was not frozen (Plate 5A). Sediment was also eroded from the upper part of the cliff face, particularly in the southern part of the scar and along the old highway; surface water is responsible for removing the loose sand and gravel (as shown by the presence of gullies and rills; Plate 5B). Areas of material gain, indicated by elevation increases (in Figure 9, coded light and dark blue), exist landward of the edge of the landslide and in the central and northern sections of the landslide scar. Low grasses and shrubs have taken root on certain parts of the landslide scar surface (Plate 5C), and the 2017 survey shows an overall seasonal increase in the height of this vegetation compared with the 2016 survey, resulting in apparent increases in the surface height locally. The non-vegetated parts of the scar show decreases of up to 1 m of elevation, suggesting that the area remains unstable and that the sediment continues to be redistributed to re-establish a stable angle of repose.

2007 Landslide

Compared to the 2013 landslide, the 2007 landslide area is more stable. An examination of the 2017 and 2016 orthophotos and DSMs reveals that most of the face of the 2007 landslide scar is vegetated, and there is an increase in the height of the vegetation at the time of the 2017 survey compared to the 2016 survey (Plate 5C, D). The scar is sta-

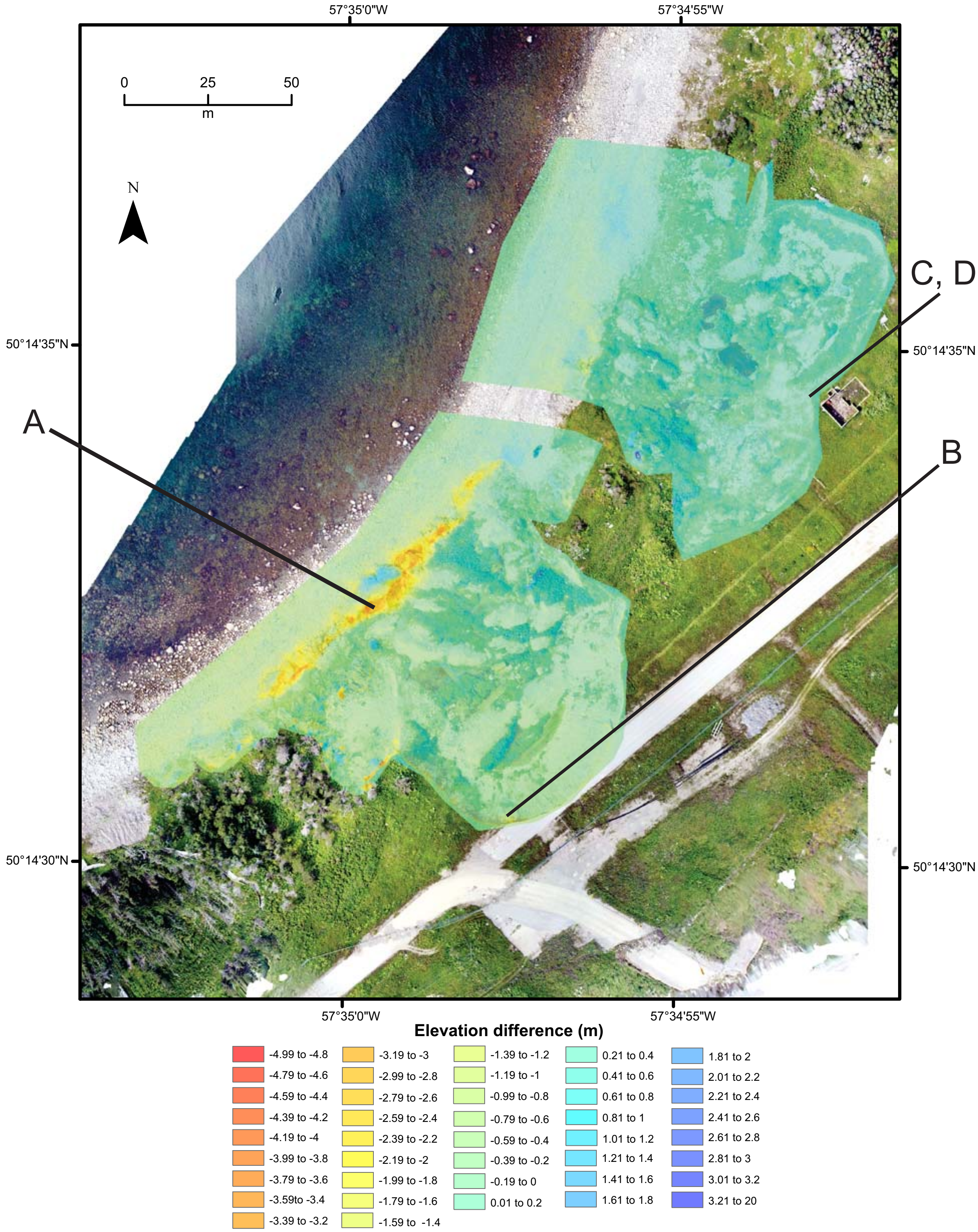

Figure 9. *Orthophoto showing elevation difference between the 2016 and 2017 UAV flights for Daniel's Harbour. The magnitudes of elevation change are represented by a colour-coded scale; positive values denote elevation gain, and negative values denote elevation loss. Dark blue indicates areas of significant elevation gain, light blue indicates minimal elevation gain, yellow minimal elevation loss and red indicates significant elevation loss. The labels A–D refer to the locations of the images in Plate 5.*

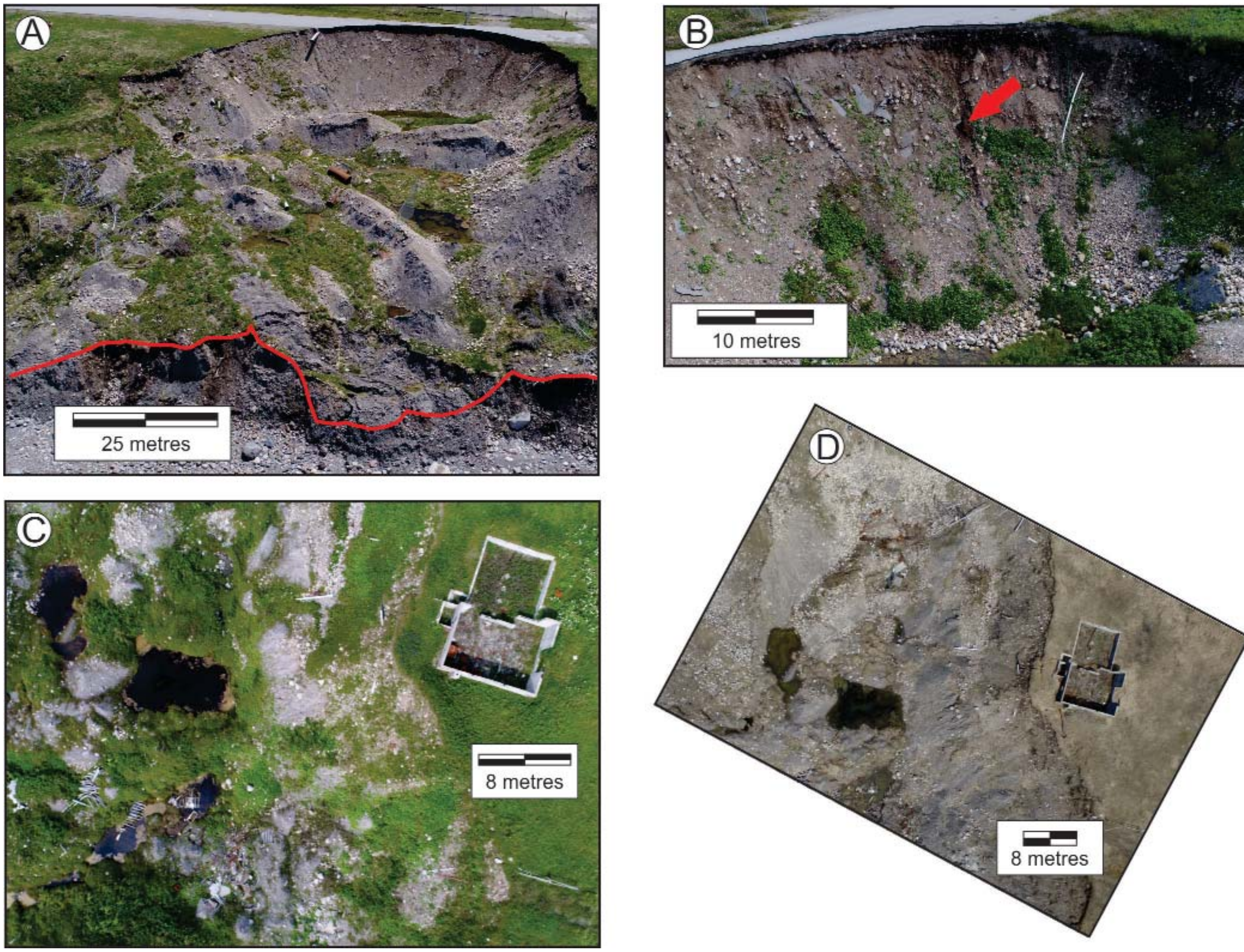

Plate 5. *An examination of the images captured by the UAV of Daniel's Harbour site and field-based observations led to the indication of factors resulting in elevation change; these are described in Plate 5A–D. Image location is identified by the corresponding letter on the orthophoto in Figure 9. Images A and B were taken at a 90° angle relative to the cliff, and images C and D were taken straight down. A) Image of the landslide and beach. Waves have removed sediment from the base of the cliff, as evident from the notch outlined in red; B) Image of the top of the landslide. The passage of surface water over the face of the slope has dislodged sand down the slope towards the base of the cliff, resulting in the formation of gullies (red arrow) and rills; C) Image of the landslide area, taken in 2017; D) Same portion of the cliff face as in C, photographed in 2016. The vegetation was higher in 2017 than in 2016, contributing to an increase in the apparent surface elevation.*

ble because vegetation has had time to re-establish, with roots reinforcing the soil's shear strength (Irvine, 2015). Non-vegetated portions of the landslide scar also show increases in ground elevation between the two surveys. An examination of the orthophotographs from 2017 and 2016 indicates that cobbles on the surface of the landslide moved vertically but not horizontally; the displacement of cobbles and subsequent gain in ground elevation is due to frost heave. During the winter, water in the soil may have frozen, formed ice lenses, and the ground surface heaved (pushed) upward. During spring thaw, when the ice melted, the voids created by the ice lenses have been infilled by fine-grained sediment, resulting in the cobbles remaining in the raised position. Future UAV surveys of the Daniel's Harbour area will focus on testing this hypothesis.

PARSON'S POND

The difference in DSMs from 2017 and 2016 indicates that overall, the cliff face has lost volume, which is consistent with field observations of erosion and changes in the position of the clifftop (Figure 10). By comparing the DSMs with field observations and images captured by the UAV, processes leading to erosion were identified (Plate 6).

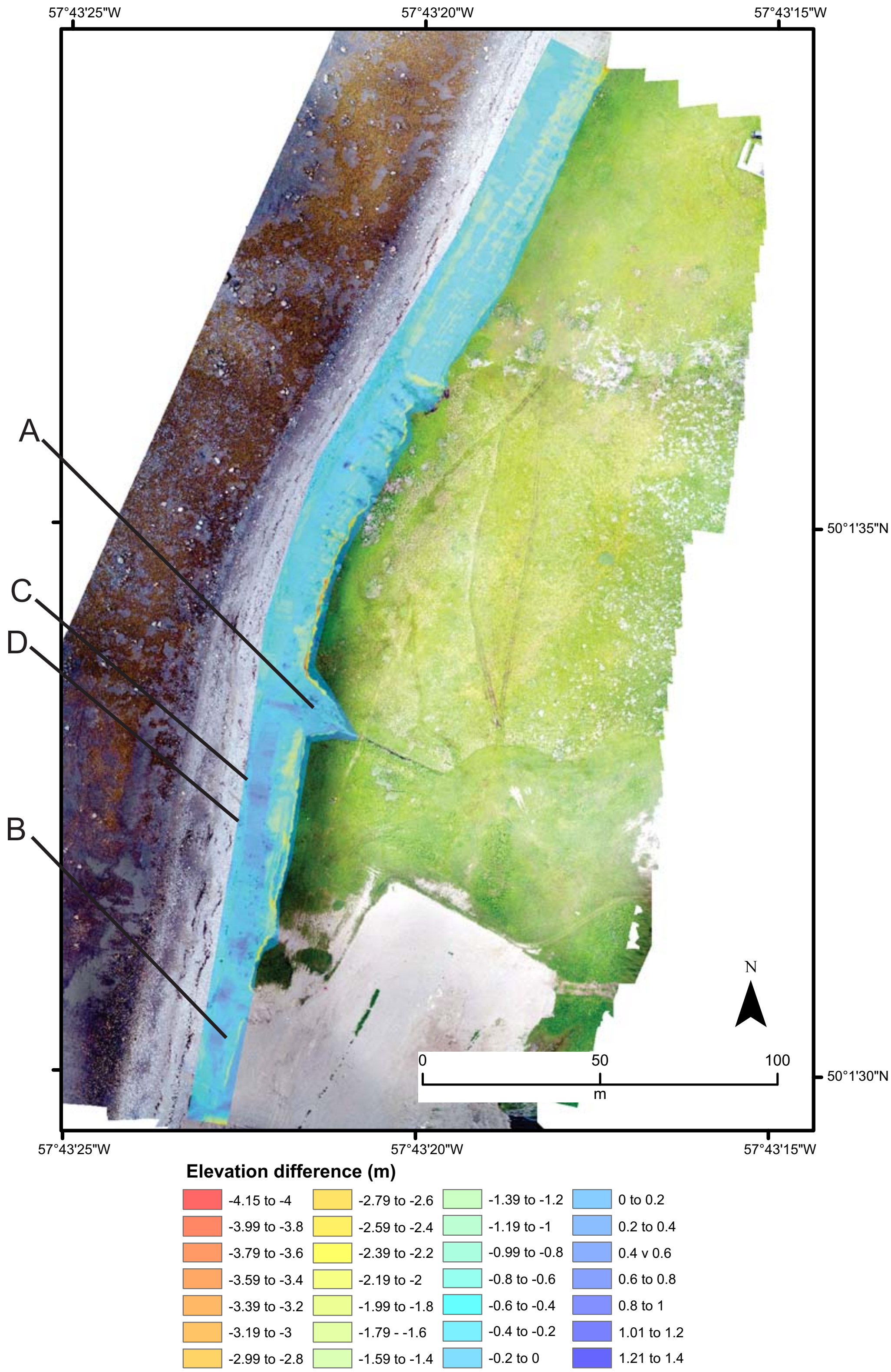

Figure 10. *Orthophoto showing elevation difference between the 2016 and 2017 UAV flights for Parson's Pond. The magnitudes of elevation change are represented by a colour-coded scale; positive values denote elevation gain, and negative values denote elevation loss. Dark blue indicates areas of significant elevation gain, light blue indicates minimal elevation gain, yellow minimal elevation loss and red indicates significant elevation loss. The labels A–D refer to the locations of the images in Plate 6.*

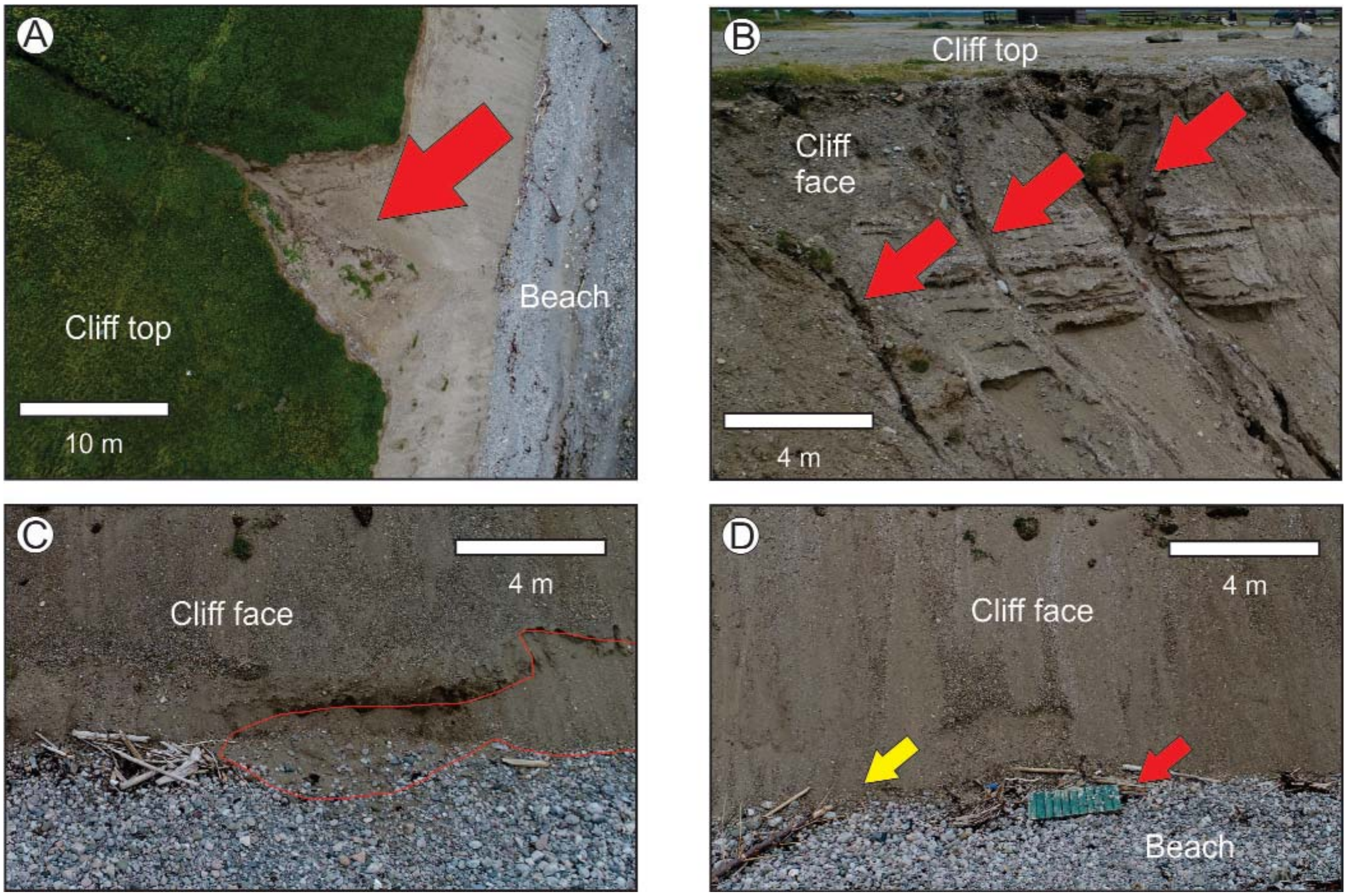

Plate 6. *An examination of the images captured by the UAV and field-based observations at Parson's Pond led to the indication of factors resulting in elevation change, and are described in Plate 6A–D. Image locations are identified by the corresponding letters on Figure 10. Images B–D were taken at a 90° angle relative to the cliff; the camera was oriented vertically for image A. A) In topographic lows landward of the cliff edge, water is being concentrated. When the flow of water reaches the cliff edge, sand, silt and gravel are carried downslope, resulting in the formation of large gullies (red arrow); B) Image of the cliff face. The passage of surface water over the face of the slope has dislodged sand, silt and gravel down the slope toward the base of the cliff, resulting in the formation of gullies (red arrows) and rills; C) Image of the base of the cliff and beach. Waves have removed sediment from the base of the cliff, as evident from the notch outlined in red; D) Image of the base of the cliff and beach at a different location from C. Here, there is no evidence of wave-based erosion, such as wave notching; unconsolidated sediments eroded from the cliff have formed a fan (yellow arrow), and waves have deposited driftwood and debris (red arrow) along the base of the cliff.*

In areas of low elevation, landward of the cliff edge, surface water is preferentially diverted toward discrete gullies in the cliff face (Plate 6A). The surface water flowing over the cliff face removes the sand, silt and gravel (Plate 6B). The gullying, rills and piping indicate that surface and groundwater are influential agents in erosion. As in the scar from the 2007 landslide at Daniel's Harbour, portions of the toe of the slope have been losing sediment at an accelerated rate compared to the rest of the slope face; waves are likely removing sediment during storms (Plate 6C). Along much of the cliff base, colluvial material is present, indicating waves have not moved this material since its deposition, they have, however, deposited driftwood (Plate 6D). Both of these observations suggest that waves are not contributing significantly to erosion. There is an increase in elevation in small pockets on the cliff face, similar to Daniel's Harbour, landward of the top of the cliff; this is due only to an increase in the height of the vegetation during the 2017 survey, compared to 2016.

GEOPHYSICAL RESULTS

DANIEL'S HARBOUR

Figure 11 displays the GPR profile collected on line DH-01 at the Daniel's Harbour site and the contoured section of inverted resistivity from the DCR survey on the same line.

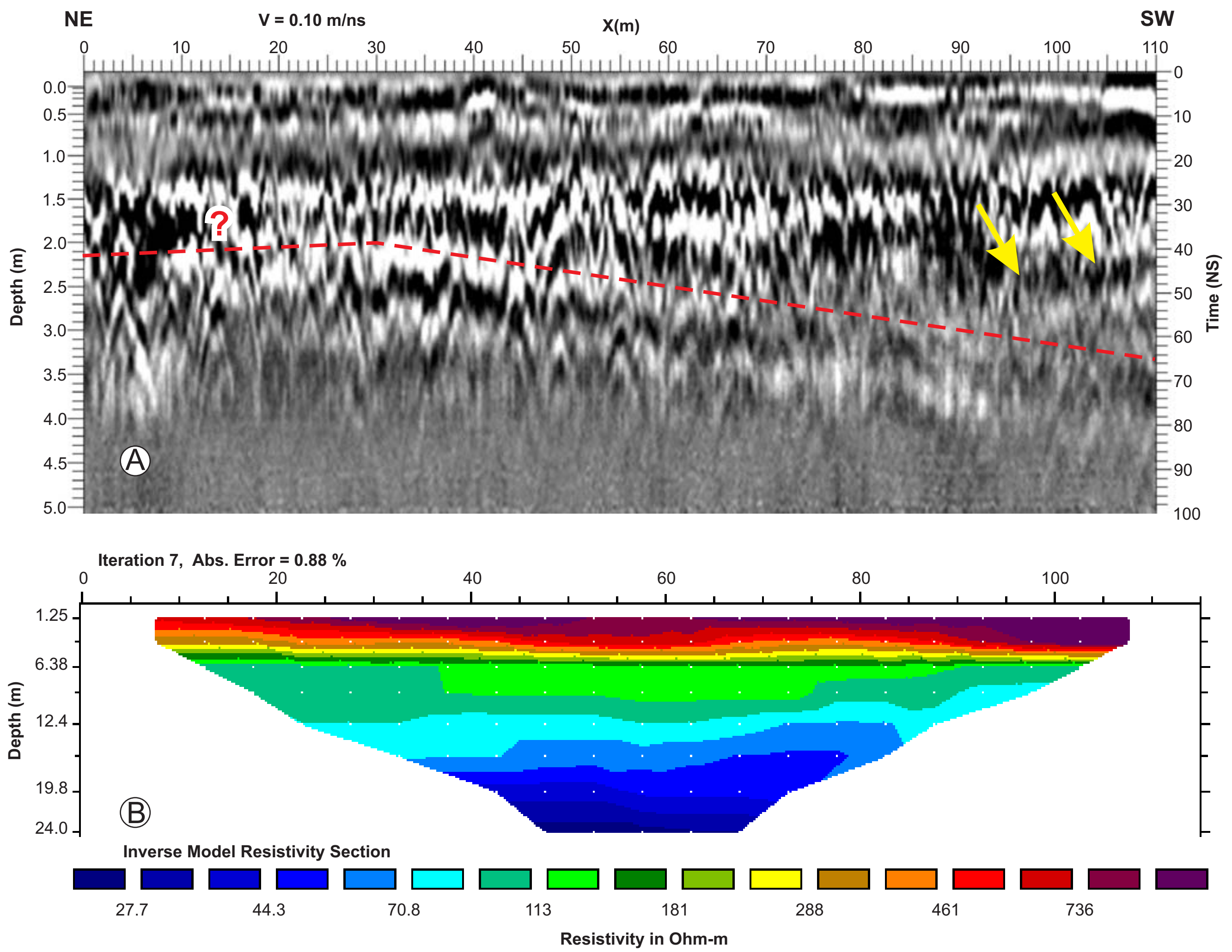

Figure 11. *A) The GPR profile from line DH-01 at the Daniel's Harbour landslide site. Vertical exaggeration has been applied to emphasize near-surface features. Background subtraction and "dewow" filtering were applied. The dashed red line is the inferred interface between sand and gravel above, and diamicton below. The yellow arrows indicate an overlying interface perhaps related to the water table; B) Corresponding DCR inverted section. A logarithmic contour interval is used. The depths on the vertical axis correspond to the centres of the inversion cells. The data presentation is oriented northeast to southwest, looking southeast.*

Inversion modelling of the apparent resistivity section for this site resulted in a resistivity model that fits the data to within a few percent, after only a few iterations. The inverted section, Figure 11B, shows a sharp, flat interface between a top layer of relatively high resistivity, and a moderately resistive middle layer. In this section, the steepest resistivity change is between depths of 3.8 and 6.4 m (yellow contour interval). There is a pattern of increasing resistivity within the top layer toward the southwest, *i.e.*, with increasing values of x, and a decrease in resistivity with depth.

Apparent chargeabilities (IP) were recorded with the DCR line DH-01 survey, for all arrays within the electrode spread. However, due to the presence of a resistive near-surface layer and the power limitations of the instrument, deviations in the chargeability measurements were too high for the IP surveys to be considered reliable, particularly for the deeper readings (larger b-spacing of current electrodes). Inversion modelling of chargeability was attempted using RES2DINV, but, as anticipated, the chargeability profile generated was extremely noisy, and could not be rationalized in terms of the geological setting. The chargeability results are not presented here.

After Schlumberger modelling using VES software, and data from various locations near the centre of the DCR survey (x approximately 50 to 65 m), it was determined that a

3-layer model fits the data (with a least squares misfit of 3–4%) better than a 2- or 4-layer model. For the best-fit VES models, the interpreted thicknesses of the uppermost two layers are about 4.8 m and 16 m, respectively. These thicknesses are comparable with borehole data, which give thicknesses of 2 to 4 m for the marine veneer of loose sand and gravel (coded as SM in Table 4); and 17 m of the compact marine diamicton (SC–SM and SC in Table 4). The modelled resistivities of the layers are distinct, being 900 ohm.m (Ω·m) and 70 Ω·m for the first two layers, and 26 Ω·m for the (indefinitely thick) lowermost layer.

Figure 11A displays the GPR profile collected over the corresponding DCR line at the landslide site. The section is characterized by many crossing, sloping reflections caused by scattering of the radar pulses from cobbles distributed through the near surface. These reflections are so concentrated that isolating individual hyperbolae for precise velocity modelling (*see* Processing) was difficult. However, a wave velocity of 0.10 m/ns was estimated from one hyperbola, and this value was used to scale the profile with depth in Figure 11A.

The pattern of light and dark bands at very shallow depths (<0.5 m) records the direct arrival of the 'ground wave' that travels along the surface of the ground between the antennae. Variability observed in this signal is likely related to changes in the roughness and composition of the surface. Reflections are not discernible beyond a depth of approximately 4–5 m (Figure 11A). Despite the scattering at shallower depths, an interface is detected at 2 to 3 m depth. This interface, which must be associated with a change in dielectric properties, could be the boundary between the marine veneer and the diamicton, or it may be the water table, which overlies the diamicton layer, or even related to an increase in clay content – or it may be a combination of these factors. Toward the southwest, the interface splits, with one reflection sloping downward and the other sloping gently upward (yellow arrows). Possibly the lower reflection is the top of the diamicton layer and the upper reflection is the water table or a lens of more clay-rich gravel.

If the interface is the veneer-diamicton boundary, the GPR data suggest that the unit of near-surface gravel is 2–4 m thick, and is cobble-rich. This corresponds to the range of thicknesses recorded in boreholes (Table 4). In particular, the borehole data for BH6 (closest to this DCR line, Figure 3) suggest that the sand and gravel layer is 2.6 m thick in this area. Both borehole and GPR data indicate that the gravel layer thickens to the southwest, possibly due to increased coastal erosion and weathering of the diamicton layer.

The inverted DCR profile shows an increased resistivity toward the southwest, in accordance with a thickened layer of resistive gravel. There is a difference of approximately 1 m in the estimates, from the DCR and GPR data, for the depth to the veneer-diamicton interface. This discrepancy can be attributed to uncertainties in the wave velocities of the GPR signal, and to resolution limitations in the DCR modelling. The RES2DINV models assume a constant resistivity in each inversion cell, and the VES models assume sharp changes in resistivity at layer interfaces and a

Table 4. Unit thicknesses from borehole data at the Daniel's Harbour site; unit thicknesses and average resistivities estimated from geophysical sections and VES modelling

Material	*Borehole Thickness (m)	Thickness (m) DCR Inversion	Thickness (m) VES Modelling	Approximate Resistivity (ohm-m)	Interpreted Genesis	Borehole Code
Loose sand and gravel	2.6	4-6	5	900	Marine veneer (nearshore sediments)	SM
Compact to dense grey, silty clayey-sand	9.9	14-17	16	70	Marine diamicton (till)	SC-SM
Loose to compact clayey-sand with gravel - occasional cobbles	9.5				Marine diamicton or marine debris (melt-out?). Emplaced in an ice-proximal marine environment	SC
Grey sandy lean clay	2.4	NA	NA	26	Marine sediments deposited by settling in quiescent waters	CL
Loose to compact clayey-sand with gravel - occasional cobbles	4	NA	NA	NA	Marine diamicton or marine debris (melt-out?). Emplaced in an ice-proximal marine environment	SC

*From Borehole 6, the nearest borehole to DCR survey line DH-01 uniform resistivity within layers. These assumptions do not fully represent the variability in the subsurface. However, there is excellent qualitative agreement between the results on the ground structure using both methods, as validated by the borehole data. The GPR data provide detailed information on the near surface complementing the deeper but lower resolution imaging of the DCR.

PARSON'S POND

Figure 12 displays the inverted DCR section and GPR profile for line PP-01 at Parson's Pond (for location, *see* Figure 2, Table 5).

The DCR inversion shows a 3-layer sequence, consisting of an uppermost conductive layer, an intermediate, more resistive layer, and another conductive layer beneath. The transition between the top and middle layers appears as a sharp interface, which slopes gently to the north, and within these layers, resistivity decreases to the north. In the centre of the section, the interface is present between depths of 3.8 and 6.5 m, remarkably similar to the transition depths observed at the Daniel's Harbour site, despite the sediment layers being different. The resistivity in the third layer changes gradationally between depths of 16 and 24 m. A gully in the surface topography, about 1.5 m deep and having raised shoulders, exists at x=65–70 m (*see* Plate 6A) and may be partly responsible for more variable resistivity data recorded in this part of DCR line PP-01.

Apparent chargeabilities were recorded and modelled for DCR line PP-01, but as with line DH-01, the results were far too noisy to interpret, or to provide insight into subsurface stratigraphy.

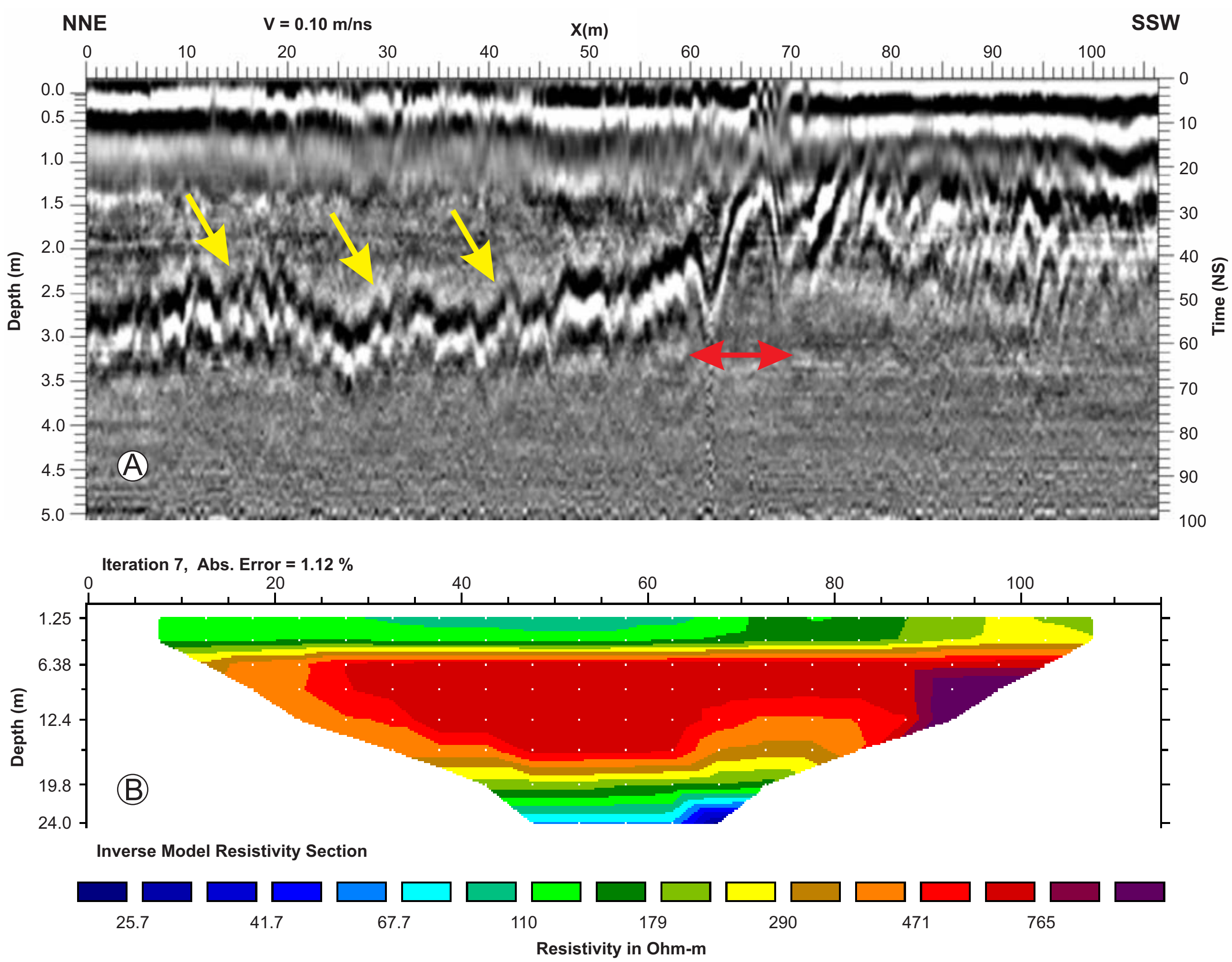

Figure 12. *A) The GPR profile from line PP-01 near Parson's Pond. A wave velocity of 0.10 m/ns was obtained from a hyperbola at the ~2.5 m interface, which is indicated by the yellow arrows. Red double-headed arrow indicates the location of a gully in surface topography. For data processing, see caption for Figure 11A; B) Corresponding inverted resistivity section from DCR data. Orientation of the line is north-northeast–south-southwest.*

Table 5. Unit thicknesses estimated from coastal sections at the Parson's Pond site, and thicknesses and average resistivities estimated from the inversion section and VES modelling of DCR data from line PP-01

Material	Thickness (m) Estimated from Coastal Exposures	Thickness (m) DCR Inversion	Thickness (m) VES Modelling	Approximate Resistivity (ohm-m)	Interpreted Genesis	Layer Code
Loose sand and gravel with cobbles	5	4-6	4.7	110	Marine nearshore sediments	SC
Well-sorted sands coarsening up to gravel	>13.5	14-16	13	640	Ice-contact delta	S
Unknown. No exposure	NA	NA	NA	20-200	Unknown - bedrock(?)/till(?)	?

The VES modelling of data from the centre of the survey (x = 57.5 m) produced a best fit model (with a misfit of approximately 4%) consisting of three layers, and having resistivities, from top to bottom, of 110, 640 and 20 Ω·m. The model thicknesses for the first two layers were determined as 4.7 m and 13 m, respectively.

Figure 12A displays the GPR profile for PP-01. The dominant feature is a sharp but irregular interface, defined by prominent reflection (yellow arrows). It extends northward from about x=75, descending from near the surface to a depth of about 3 m. The apparent peak-and-trough structure in the interface at x=60–70 is the result of the change in surface elevation associated with the gully mentioned above. The low amount of scattering within this top layer indicates that only sparse cobbles and boulders are present. The different physical properties and texture suggest that it is a different material – *e.g.*, soil or clay – from the sand and gravel encountered in the top layer at Daniel's Harbour.

From x=75 onward, the near-surface material transitions rapidly from hard-packed soil into, what appears to be, a sandy gravel similar to that observed at Daniel's Harbour. Surface features along PP-01 are consistent with the subsurface image: from x=0 to 75 m, the ground is densely vegetated with grasses and shrubs, whereas, from x=75 m onward, the ground is markedly different: sandy, and with sparse vegetation.

Based on its relatively high resistivity, it is believed that the material below the interface in the GPR profile is a sand/gravel layer. The interface itself is characterized by many diffraction hyperbolae, likely produced by a layer of cobbles. The GPR profile does not show reflections at deeper levels, beyond this accumulation of cobbles.

The UAV photographs taken along the nearby coastline (Plate 3) shows stratigraphy that corresponds well with the uppermost two layers modelled from DCR data. There is a dark, relatively cohesive top layer, which may be clay-rich, over more friable delta sands. The estimated thickness of the top layer is approximately 5 m, thicker than that observed in the GPR data (up to approximately 3 m) but similar to the results of the DCR modelling. The top layer is underlain by an irregular pavement of cobbles, and is underlain by thick sequences of relatively well-sorted delta sands.

The lowermost layer, detected in the DCR results and characterized by very low resistivity, has not been identified in coastal cliffs in this area; the 20-m-high coastal cliff exposures show only delta sands, extending to the beach level. The low resistivity modelled at depth on the DCR resistivity section may possibly be related to salt water incursion, or to the existence of a clay-rich sediment layer or a conductive rock, which is not exposed.

Additional GPR lines were surveyed adjacent to line PP-01 at Parson's Pond (Figure 2, Table 1) to test the lateral continuity of features modelled by the DCR survey, and to test the utility of the GPR method over terrain, where DCR surveying is problematic (*e.g.*, where significant slope changes exist).

Figure 13A displays the GPR profile for line PP-02, which starts at the end of line PP-01 and extends in a southerly direction. Location markers, labelled F4 to F6 on the profile, were chosen at inflection points in the ground slope along the traverse. The first location marker (F1) was chosen at the start of the line, over the southernmost electrode of the DCR array on line PP-01, and the final location marker (F7) marked the end of the line, adjacent to the parking area, 135 m to the south. These locations were recorded in the GPR data by the operator during acquisition, and their GPS positions were accurately determined by the RTK system (*see* Figure 2, Table 1).

The ground from x=0 to x=28 m consists of semi-compact sand and sparse vegetation; for the remainder of the

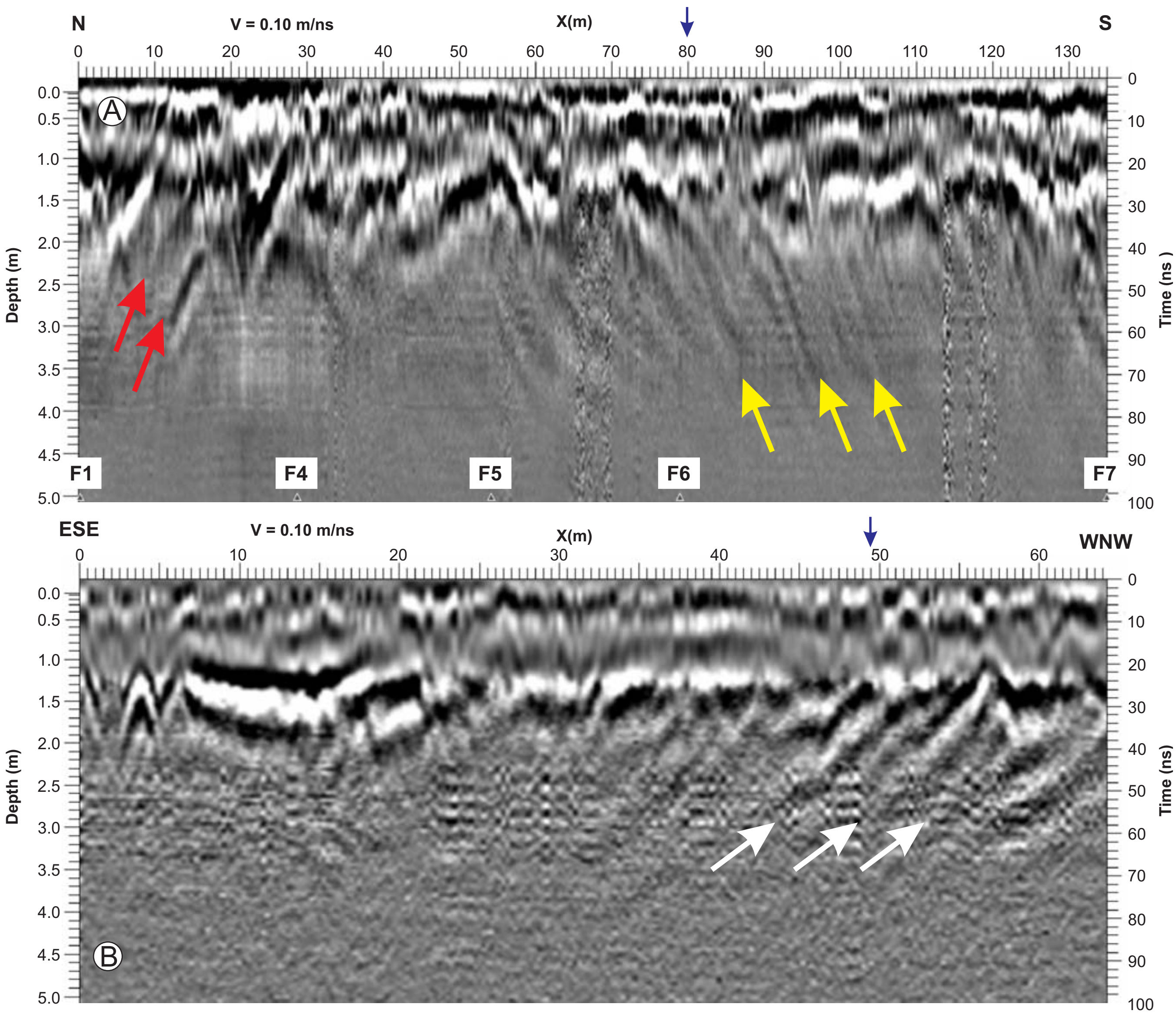

Figure 13. *Profiles from GPR data recorded to the south from DCR line PP-01 at Parson's Pond. A) Line PP-02 is a north-south traverse, starting from the top of a ridge and continuing down slope into an adjacent, unpaved level area adjacent to the rest-stop parking; B) Line PP-03 is a perpendicular, east-southeast to west-northwest traverse recorded across the widest portion of the graded area. Blue arrows at the top of each profile indicate the locations of intersection of these two GPR lines. A radar pulse velocity of 0.100 m/ns was assumed in processing both profiles, consistent with that used for adjacent profile PP-01 (Figure 12A). Note the difference in horizontal scales – the vertical exaggeration for line PP-02 is approximately x10, whereas that for PP-03 is approximately x 6. Red, yellow and white arrows indicate the locations of apparent dipping reflectors at depth, various directions.*

line, the surface material appears to be recently worked gravel, as it is not vegetated. The interval from x=18 to x=28 m was recorded along a steep downward slope; from x=28 m to the end of the line, the terrain varies from flat to sloping gently upward to the south.

The profile shows a very irregular interface at a depth of about 1 m. The layer above this interface may represent non-layered material used during the construction of the rest-stop parking area. At depth on this GPR profile, beginning at x=42 and onward, more subtle south-dipping reflections (yellow arrows, Figure 13A) can be observed. These features are interpreted to be delta foreset beds, as observed in nearby coastal exposures (Plates 2 and 3). Due to the attenuation of the GPR signal with depth, the foreset beds are only detectable to a depth of 3.5 m. In Figure 13A, the dips of these reflectors appear steepened, due to the vertical exaggeration in the profile. An average apparent dip of approximately 13° was determined for the features indicated by the yellow arrows.

Between x=12 and x=18 on GPR line PP-02, at a depth of 2 to 3 m (red arrows, Figure 13A), there appears to be a reflection interface resembling a foreset bed dipping northward; *i.e.*, in the opposite direction. The apparent dip of this reflector is uncertain, however, as this portion of the profile was recorded while traversing down slope; *i.e.*, with decreasing elevation in the x direction.

An east-southeast–west-northwest-oriented GPR line, PP-03 (Figure 13B), was recorded over the unpaved area adjacent to the rest stop, intersecting GPR line PP-02 at x=80 m. The surface material was loose gravel with no vegetation. This area appeared to have been recently graded – the ground surface on this line was uniform and sloped gently downward to the west. The GPR profile for line PP-03 is similar in appearance to the central and southern parts of line PP-02 (Figure 13A), and shows a prominent reflector at 1.2 m depth. From approximately x=7 to x=20, this reflection is particularly flat and distinct – this part of line PP-03 is located over a former building foundation that has since been infilled with gravel. Since the layer above this prominent reflector is nearly devoid of features, it is interpreted to be composed of gravel used for construction. In the western half of GPR profile PP-03, several subtle reflectors can be observed, at depths of 2 to 4 m, dipping to the east (white arrows, Figure 13B). These dipping reflectors are similar in appearance to features on line PP-02, so they are interpreted as delta foreset beds, but with only 7° of apparent dip to the east. Therefore, delta foreset beds are interpreted to underly the area near the rest stop, and they appear to dip gently toward the southeast.

SUMMARY

Coastal erosion rates can be efficiently calculated by analyzing, gridding and comparing UAV imagery acquired in successive aerial surveys. Differences in DSMs generated from multi-year high-resolution airphotos allow for identification of discrete areas that are actively eroding or accreting. In addition, the imagery is very useful in identifying glacial stratigraphy in inaccessible areas (*e.g.*, rugged coastline, steep cliff exposures). The detail captured in the photographs elucidates geological features (*e.g.*, clay lenses, Parson’s Pond) that can be overlooked during ground investigations. By comparing temporal changes in elevation with glacial deposits, linkages between sediment type and susceptibility to erosion can be inferred. The images can also assist in understanding the depositional environment, and in the classification of geological layers.

Direct-current resistivity was successful in discerning differences in the glacial sedimentary succession at Daniel’s Harbour and Parson’s Pond. The quartz-rich sands in ice-contact deltas at Parson’s Pond are highly resistive (Figure 12B), whereas the clay-rich diamictons at Daniel’s Harbour are moderately to highly conductive (Figure 11B). Furthermore, depths to layer interfaces estimated from DCR profiles agree with sedimentary layer thicknesses measured from boreholes; the thicknesses of resistive layers in the profiles closely approximate those of the sandy, marine veneers at Daniel’s Harbour, and the conductive layers were similar in thickness to the sandy, clay-rich marine diamicton (Table 4, Figure 11B). More importantly from a hazard perspective, the DCR profiles identified the presence of a discrete, conductive clay layer underlying the marine diamicton at Daniels Harbour (Table 4, Figure 11B) at depths to 25 m.

Ground-penetrating radar was less successful in delineating both the differences and thicknesses of sedimentary layers in both areas, due to loss of signal strength and scattering of the signal by large boulders and cobbles in the subsurface. However, GPR proved useful in approximating the thickness of the uppermost subsurface layers, especially in areas where boulders and cobbles were absent from the subsurface (*e.g.*, prominent reflections down to a depth of 2 m between x = 80 and x=64 on Line DH-01, Figure 11A). The GPR was also successful in delineating the paleosurface of the marine diamictons underlying the sandy nearshore-marine sediments, and illuminating the delta foresets at Parson’s Pond (Figure 13, Plates 2 and 3).

CONCLUSIONS

The UAV and geophysical surveys carried out near the communities of Daniel’s Harbour and Parson’s Pond were successful in identifying areas of potential landslide risk.

1) Repeated aerial surveys using camera-mounted UAVs have measured temporal changes in surface elevation and successfully identified areas that have experienced material loss and gain.

2) High-resolution imagery of coastal cliffs is invaluable in determining the distribution of glacial deposits in areas that are difficult to access and can be used to identify failure-prone layers (*e.g.*, clay units, layered cobbles and sandy units surrounding diamictons).

3) Direct-current resistivity (DCR) surveys are effective in differentiating between clay-rich and clay-poor environments, and are therefore useful in the identification of clay layers, that have been previously associated with landslides.

4) Using a 5-m-electrode spacing and resulting 115 m spread, the inversion of DCR results is effective in approximating the thicknesses of sedimentary units to depths of 24 m, sufficient to image the clay layer underlying marine diamicton at the Daniel`s Harbour site.

5) Ground-penetrating radar (GPR) was moderately successful in delineating the paleosurface of the marine diamictons, within a few metres of the surface, even though cobbles and boulders were present in the uppermost sediments.

6) The GPR was successful in imaging the subsurface structure of delta foreset bedding to a depth of about 4 m at Parson's Pond.

FUTURE WORK

The preliminary results from the application and testing of the geophysical methods at Daniel's Harbour suggest that DCR and to lesser extent, GPR could be successfully used to determine subsurface stratigraphy in other known hazard-prone areas (*e.g.*, Sally's Cove).

Further studies are needed to refine the geophysical interpretations, understand the triggers for landslides and to make sure that the communities can access the data from the study. They include:

1) Investigating the physical properties of glacial deposits on the west coast, to constrain geophysical models and to enable comparison of modelled resistivity values with the measured resistivities of rocks and soils present in the subsurface. This comparison will be useful to identify other environments that may contain clay and are vulnerable to landslides.

2) Given the success of DCR in imaging to a depth of 24 m, longer DCR spreads (with >5-m-electrode spacing) could be tested to image deeper. As well, shorter spreads, with 1–2-m-electrode spacing, could be tested to better resolve near-surface layers in particular, for detailed comparison with GPR surveys. Further testing of GPR surveys using longer antennae, which may potentially image deeper, would also be valuable.

3) Conducting passive seismic surveys, by setting out an array of geophones for an extended period of time, near roads around the landslide site at Daniel's Harbour to monitor traffic vibrations that are postulated as being a possible trigger for landslides.

4) Conducting active seismic surveys that involve a controlled source (*e.g.*, a hammer blow) from which seismic waves are emitted. Analysis of reflections and their arrival times may resolve fractures or displacements in the subsurface, which could lead to prediction of failure planes.

5) Presenting the data collected, from this and future surveys, clearly and convincingly to stakeholders for use in community planning.

6) Development and testing of the effectiveness of different information–dissemination methods (e.g., web-based interactive portals, hazard maps, workshops, presentations) to allow for the efficient distribution of geoscientific information to the public.

ACKNOWLEDGMENTS

Gerry Hickey is thanked for his logistical support, daily safety monitoring and efficiency and helpfulness in procuring vehicles for field-party participants. Much appreciation goes to Stephen Amor for his review of this report. Lindsay Oldham is commended for her excellent UAV piloting and survey skills; Sandra Murphy is thanked for her diligence and hard work, especially with the ground-geophysical and UAV surveys.

REFERENCES

Batterson, M., Liverman, D. and Taylor, D.
2006: Geological disasters in Newfoundland and Labrador. Geological Survey of Newfoundland and Labrador, Open File 2929, 85 pages.

Cawood, P.A., Williams, H. and Grenier, R.
1987: Geology of Portland Creek area (12I/4), western Newfoundland. Geological Survey of Canada, Open File 1435, scale 1: 50 000.

Cooper, G.R.J.
2000: VES Freeware, Ver. 1.2. Web: SGRC@ Cosmos. wits.ac

Donohue, S., Long, M., O'Connor, P., Eide-Helle, T., Pffaffhuber, A.A. and Rømoen, M.
2012: Geophysical mapping of quick clay: a case study from Smørgrav, Norway. Near Surface Geophysics, Volume 10, Number 3, pages 207-219.

Geotomo Software
2017: RES2DINV - Rapid 2-D Resistivity & I.P. inversion using the least-squares method. Installation and getting started users guide, August 2017. Web: www.geotomosoft.com

Grant, D.R.
1994: Quaternary geology of Port Saunders map area, Newfoundland. Geological Survey of Canada, Paper 91-20, 59 pages.

Griffiths, D.J.
2013: Introduction to Electrodynamics, 4th Edition. Pearson Education. Pearson. 599 pages.

Hinchey, A.M. and Knight, I.
2011: The southern Long Range inlier, Newfoundland: Evidence for early Appalachian thrusting of Paleozoic metasedimentary rocks within a Proterozoic basement massif. Atlantic Geology Abstracts, Volume 47, Number 1, page 23.

Irvine, M.
2012: Coastal monitoring in Newfoundland and Labrador. *In* Current Research. Government of Newfoundland and Labrador, Department of Natural Resources, Geological Survey, Report 12-1, pages 191-197.

2013: Coastal monitoring in Newfoundland and Labrador: 2012 update. *In* Current Research. Government of Newfoundland and Labrador, Department of Natural Resources, Geological Survey, Report 13-1, pages 43-54.

2014: Coastal monitoring in Newfoundland and Labrador: 2013 update. *In* Current Research. Government of Newfoundland and Labrador, Department of Natural Resources, Geological Survey, Report 14-1, pages 217-229.

2015: Monitoring coastal change in Newfoundland and Labrador: 2014 update. *In* Current Research. Government of Newfoundland and Labrador, Department of Natural Resources, Geological Survey, Report 15-1, pages 263-26.

Irvine, M., Roberts, G. and Oldham, L.
This volume: Assessing the applicability of unmanned aerial vehicle (UAV) data in environmental monitoring of coastal environments: St. David's, Newfounndland.

Jacques Whitford
2006: Report 1018871: Geotechnical Consultation: Daniel's Harbour Landslide Assessment. Appendices A to G.

2008: Final Report 1043400: Phase 1 Geotechnical Assessment Daniel's Harbour Landslide, pages 1-14, plus Appendices.

Jol, H.
2009: Ground Penetrating Radar Theory and Applications, 1st Edition. Elsevier Science. 544 pages.

Knight, I.
1985: Geological mapping of Cambrian and Ordovician sedimentary rocks of the Bellburns (12I/5/6), Portland Creek (12I/4) and Indian Lookout (12I/3) map areas, Great Northern Peninsula, Newfoundland. *In* Current Research. Government of Newfoundland and Labrador, Department of Mines and Energy, Mineral Development Division, Report 85-1, pages 79-88.

Lane, J.J., Haeni, F. and Watson, W.
1995: Use of a square-array direct-current resistivity method to detect fractures in crystalline bedrock in New Hampshire. U.S. Geological Survey, pages 476-485.

Levent Ekinci, Y., Türkeş, M., Demirci, A. and Erginal, A.E.
2013: Shallow and deep-seated regolith slides on deforested slopes in Çanakkale, NW Turkey. Geomorphology, Volume 201, pages 70-79.

Lundstrom, K., Larsson, R. and Dahlin, T.
2009: Mapping of quick clay formations using geotechnical and geophysical methods. Landslides: Journal of the International Consortium on Landslides, Volume 6; pages 1-15.

McCuaig, S.
2006: Glacial spillway deposits in the Gander Lake–Gambo area. *In* Current Research. Government of Newfoundland and Labrador, Department of Natural Resources, Geological Survey, Report 06-1, pages 206-219.

Murray, T. and Booth, A.D.
2010: Imaging glacial sediment inclusions in 3-D using ground-penetrating radar at Kongsvegen, Svalbard. Journal of Quaternary Science, Volume 25, pages 754-761.

Owen, J.V.
1987: Geology of the central part of the Long Range Inlier, Fleur de Lys, White Bay South District, Englee, western Newfoundland (12I/03, 12I/04). 3 maps. Scale 1:50 000. Geological Survey of Canada, Open File 1505.

Proudfoot, D.N. and St. Croix, L.
1987: Quaternary geology of the Bellburns (12I/5 and 6) map area. In Current Research. Government of Newfoundland and Labrador, Department of Mines and Energy, Mineral Development Division, Report 87-1, pages 11-21.

Reynolds, J.M.
1997: An Introduction to Applied and Environmental Geophysics, Wiley, 806 pages.

Sensors and Software Inc.
2006: pulseEKKO PRO User's Guide. Mississauga: Sensors and Software Inc.

2017: FAQ: How Can Velocity be Extracted from Hyperbolas? Sensors and Software Resources Sensors and Software Inc. Web: https://www.sensoft.ca/resources/faq/

Sharma, P.V.
1997: Environmental and Engineering Geophysics. Cambridge University Press, 475 pages.

Szymczyk, M. and Szymczyk, P.
2013: Preprocessing of GPR Data. Image Processing & Communication, Volume 18, No. 2-3, pages 83-90.

Sutinen, R.
1992: Glacial deposits, their electrical properties and surveying by image interpretation and ground penetrating radar. Geological Survey of Finland, Bulletin 359, 123 pages.

Westoby, M.J., Brasington, J., Glasser, N.F., Hambrey, M.J. and Reynolds, J.M.
2012: ‘Structure-from-Motion’ photogrammetry: A low-cost, effective tool for geoscience applications. Geomorphology, Volume 179, pages 300-314.

Williams, H. and Cawood, P.A.
1989: Geology, Humber Arm Allochthon, Newfoundland. Geological Survey of Canada “A” Series Map (2L, 12A, 12B, 12G, 12H, 12I), 1678A, scale 1:250,000.